



## Techno-economic evaluation of a gas turbine-based power, water desalination and cooling system

Morteza Zamzam<sup>a</sup>, Amin Namjoo<sup>a</sup>, Ebrahim Jahanshahi Javaran<sup>b,\*</sup>

<sup>a</sup>Department of Mechanical Engineering, Kerman Branch, Islamic Azad University, Kerman, Iran, emails: [mortezazamzam@gmail.com](mailto:mortezazamzam@gmail.com) (M. Zamzam), [namjoo@iauk.ac.ir](mailto:namjoo@iauk.ac.ir) (A. Namjoo)

<sup>b</sup>Department of Energy, Institute of Science and High Technology and Environmental Sciences, Graduate University of Advanced Technology, Kerman, Iran, email: [e.jahanshahi@kgut.ac.ir](mailto:e.jahanshahi@kgut.ac.ir) (E. Jahanshahi Javaran)

Received 8 August 2019; Accepted 4 January 2020

---

### ABSTRACT

The present research has been concerned with the techno-economic evaluation of combined power, desalination and cooling system run by the exhaust flue gases of a gas turbine in Iran. In addition to using power generated by the gas turbine, attempts were made to use the organic Rankine cycle (ORC) to recover the heat dissipated from the gas turbine and reproduce power. Choosing the appropriate technology for the combined system involving the simultaneous production of power, freshwater, and cooling based on energy and economic analysis was investigated using MATLAB software. The results showed that a multiple-effect distillation system with the freshwater price of 1 \$/m<sup>3</sup> should be used to produce the high tonnage freshwater; to achieve the proper price of freshwater, reverse osmosis applied by giving priority to the ORC power; then, GT applications have been suggested. Additionally, R123 was selected as a working fluid. According to the calculated price of the power sale, the sale of gas turbine power could be approximately 0.1 \$/kW/h. Regarding the cooling system, it should be stated that the absorption system has a low price and high cooling load production, and a compression cooling system could be used only at low temperatures.

*Keywords:* Gas turbine; Organic Rankine cycle; Desalination; Cooling; Economic analysis

---

### 1. Introduction

The energy crisis in today's world has encouraged the researchers to look for ways that can lead to the optimal use of the existing energies; so energy optimization has been proposed as a major strategy to reduce energy consumption and decrease environmental pollutants.

Meanwhile, one of the most important solutions to ensure energy optimization is the use of simultaneous production systems to increase energy production efficiency and to use fuel resources optimally. On the other hand, the capacity of freshwater production has been increased from 95.7 million m<sup>3</sup>/d in mid-2016 to 99.6 m<sup>3</sup>/d in mid-2017.

The growing demand of 4.2% in the desalination markets indicates the growing need for freshwater, which has been rising in recent years [1]. The incremental trend in the Middle East has been significant, as compared to other parts of the world. This can be attributed to the existence of rich oil and gas resources and water stresses. To provide this amount of water, fossil fuel consumption and consequently, greenhouse gas emissions associated with global warming will increase [2]. One of the solutions to reduce greenhouse gas emissions is the simultaneous production of water, electricity, and cooling. This has received a lot of attention from various researchers.

Najjar et al. [3], for example, analyzed a system that was a combination of an upper propane organic Rankine cycle

---

\* Corresponding author.

(ORC) and a gas refrigeration lower propane cycle. The upper cycle acted as a power producer which partly ran the lower cycle. The lower propane cycle had an expander supplying power to run its compressor, in addition to cooling the inlet air entering into the gas turbine engine. The results of this plan showed that the net power and overall efficiency of the integrated system at extreme conditions ( $T_a = 45^\circ\text{C}$  and  $\phi = 80\%$ ) were increased by 35% and 50%, respectively. Iaquaniello et al. [4] also investigated the effect of the concentration of solar power (CSP) on integrating the multiple-effect distillation (MED) system by applying the exhaust vapor leaving the steam turbine and reverse osmosis (RO) system using the power generated through the turbine. Due to the reduced environmental impacts, this comprehensive system was implemented using solar energy. The results of this plan showed that the use of this method caused a reduction in freshwater production costs. Manesh et al. [5] also produced water and power simultaneously in a steam network. In this study, an analysis of exergy economics was performed to better understand the integration of the relevant cycles and to ensure the optimal connection of MED-RO water-desalination system components. Further, Mokhtari et al. [6] selected a gas turbine to respond to water and electricity demand for a region in the Persian Gulf. Due to the MED system's inability to supply the region water, the hybrid MED-RO desalination system was used. The obtained results showed that by using the gas cycle surplus power and the condenser water return of MED for the RO system, the cost of water production by the desalination system could be reduced. Additionally, using 3E analyses, Mokhtari et al. [7] investigated the production of freshwater by MED technology and solar energy to reduce the environmental impacts of freshwater production by reducing fossil fuel consumption. Loutatidou and Arafat [8] also employed the low-enthalpy heat sources to propose solutions for the production of freshwater using the MED and RO technology in the Persian Gulf region; according to the results of this analysis and the investigation of the leveled cost of water economic parameter, the proposed plan was selected. Filippini et al. [9] also integrated the MED and RO system and used the MED system output for the RO system. The results showed that, based on this integration, the lowest energy consumption could be obtained for a seawater desalination system. Based on the development of the R\_curve tool, Salimi and Amidpour [10] also investigated how the RO and MED system was selected in a simultaneous water, electricity, and heat production network. In this study, the integration of different desalination systems into the cogeneration systems was examined. Based on the operating conditions of the cogeneration system, this integration could result in either the improvement or impairment of the cogeneration efficiency. In addition, Ud-Din Khan [11] studied a nuclear power plant producing freshwater. In this analysis, which was conducted based on a technical and economic evaluation, various methods of integrating the MED + RO and (MSF - multi-stage flash) MSF + RO freshwater production systems were investigated and the results of each scenario were compared technically and economically. Ihm et al. [12] also studied MED, MSF and sea water reverse osmosis water desalination systems in a combined cycle power plant (CCPP) cycle and compared them from

an energy consumption perspective. The results showed that the CCPP with the MED system could outperform (19.3–19.5 PR) the RO system. Based on economic indices, Arani et al. [13] also investigated the economic analysis of a plant for the simultaneous production of water and electricity by considering the availability of a desalination system. Further, Hosseini et al. [14] studied the environmental optimization of the combined water and electricity production cycle. By using the genetic algorithm in this cycle, they reduced the environmental impacts of gas turbines and freshwater production. The optimization results showed that the cost of products and the environmental cost impact could be reduced by 13.4% and 53.4%, respectively, whereas a 14.8% increase was found in the total exergy efficiency. Likewise, Sanaye and Asgari [15] investigated the multi-objective analysis and optimization for power and freshwater production unit based on MSF. Their two-objective optimization was based on the reduction of environmental impacts, particularly  $\text{NO}_x$  emissions, as well as the reduction of the system investment cost. The genetic algorithm with heat recovery steam generator (HRSG) design, as well as the MSF system parameters, could improve the objective functions. On the other hand, Ghorbani et al. [16] analyzed a process of liquefied natural gas production, carbon dioxide separation, liquidation, and freshwater production. Based on the exergy analysis, the results showed that the most exergy destruction belonged to the cycle required for shell and tube exchanger and the MED system could have a gain output ratio (GOR) of 2.87 in its best condition. Ghorbani et al. [17] also developed a combined power, heat, and freshwater production system using solar energy and the Kalina cycle. This research was carried out for a residential complex in Assaluyeh at a margin of the Persian Gulf. In this study, solar energy was used to generate heat and launch the Kalina cycle, and the generated heat was used to launch a MED system. Further, Mehrpooya et al. [18] conducted the thermodynamic and economic evaluation of a combined cooling and water desalination system using solar energy. The results of the economic analysis showed that the return on the capital of this system was 5.738 y. Shahzad et al. [19] also proposed a combination of absorption and RO systems based on water restriction in the Persian Gulf region; based on heat sources, the low temperature of the industries or the use of sun caused the proposed system to have the highest efficiency of 81% and the energy consumption of  $1.76 \text{ kW/h/m}^3$ . On the basis of a solar cycle connected to a Rankine cycle, Azhar et al. [20] produced power, freshwater, and cooling in an integrated way. This system worked based on industrial heat, solar energy, geothermal energy, and ocean thermal energy. The ocean thermal energy conversion (OTEC) was interconnected with the desalination system, producing 30.49 kW with 0.73% energy efficiency. The proposed system was analyzed energetically and exergically, showing that the energy and exergy efficiencies of the overall system were 13.93% and 17.97%, respectively. Nemati et al. [21] used heat loss from a large diesel engine on a ship for seawater desalination. Based on the beam boundary in the performed optimization, the efficiency of the collection was calculated to be 37% and the cost of exergy destruction was obtained to be 60 \$/GJ. Najjar et al. [22] also performed thermo-economic analysis and optimization of a novel inlet

air cooling system with gas turbine engines using cascaded waste-heat recovery. In this work, optimization, by using the direct search method and the EES Software, resulted in a final value of  $\eta_{\text{Thermal}} = 28.34\%$ . Furthermore, a sensitivity study was carried out, showing a drop of 10% in the operating variables and its effect on the total operating cost.

The shift from using fossil fuels to the simultaneous production of electricity, freshwater, and cooling in gas turbines requires a serious study to minimize the amount of pollutants involved in it. In fact, according to the change that has occurred in this approach, the purpose of this research was to use the ORC in addition to the power generated by the gas turbine to recover the waste heat of the gas turbine for power regeneration. Other objectives of this study have been the analysis and determination of the optimum water desalination system using RO and MED methods, as well as the determination of the proper method of cooling production using absorption and compression methods and their investigation in terms of economy.

The optimal design of this research has been proposed to take advantage of some of the mentioned benefits. To the best of the author's knowledge, there is no published work regarding the optimization of the combined power, cooling and freshwater production system using gas turbine and ORC, absorption, and RO and MED methods simultaneously.

## 2. Methodology

### 2.1. System description

Fig. 1 shows various components of the combined cooling, power and water (CCHPW) cycle. The schematic

diagram of the systems in Fig. 1. In this figure, which is based on the MAN gas turbine (Oberhausen, Germany), THM 1304-11 model, the NGL refinery of Siri Island, Iran, the electricity generated for cooling or freshwater production was used. The output heat in a heat exchanger was given to vapor or organic fluid. The produced vapor either entered into a thermal desalination device, producing freshwater or went into a single-effect absorption chiller. If the heat is exchanged with organic fluid, the organic fluid enters into a turbine or expander. In this case, on the one hand, both power and the organic fluid which had lost its energy could exit the turbine and continue the Rankine cycle.

The produced power either enters into the refrigeration cycle, producing cooling or causes the RO system pump to rotate and increase water pressure; based on the osmotic theory, which is further explained in this study, pressurized saline water is transmitted through membranes, producing freshwater. The above-mentioned system is composed of two main parts. The first part includes the energy leading to electricity generation, and the second one consists of the energy existing in the exhaust gas from the gas turbine in the surplus heat of the system. In both parts, the goal is to produce cooling and freshwater, but different technologies are used in each of them. This has been one of the goals of this study from a technical and economic point of view. Finally, it is found which technology can lower the costs and increase the produced cooling and water tonnage. In this analysis, which is done using the MATLAB software, three scenarios have been investigated and for each one, an optimal cycle has been presented.

*First scenario:* production of high freshwater tonnage, low-temperature cooling, and electricity sale to the network;

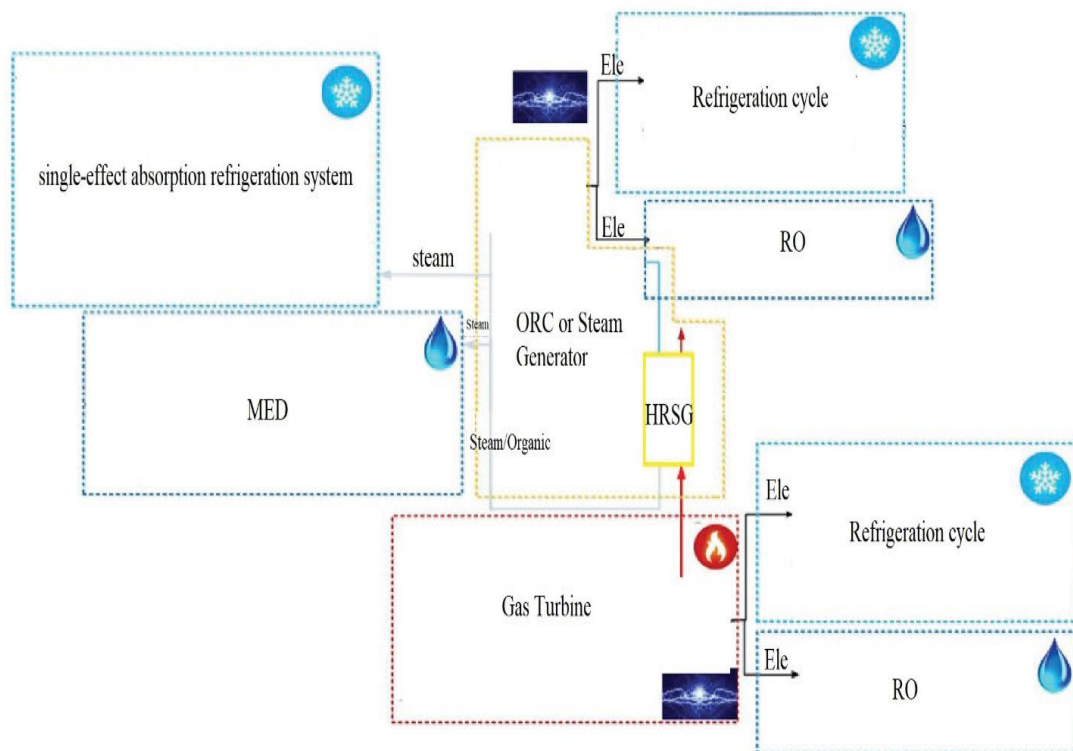


Fig. 1. Schematic of the simulated CCHPW cycle.

second scenario: reasonable price for freshwater and low-temperature cooling with high cooling tonnage together with electricity sale; third scenario: high freshwater tonnage at a reasonable price and high cooling tonnage and electricity sale to the network.

Finally, Fig. 2 shows the flowchart for the various cycles of the studied combined system. How this flowchart works and the way the appropriate system is selected can be seen in Table 18 and Figs. 26–28.

2.2. System modeling

2.2.1. Gas turbine cycle modeling heat recovery boiler design

GT model MAN gas turbine, THM 1304-11 model, was simulated for the site conditions, in the south of Iran, Siri Island, close to the Persian Gulf. According to Fig. 1, the schematics of the combined gas turbine and HRSG system can be seen in Fig. 3.

In the present work, natural gas was considered as the fuel of the plant. Table 1 represents the inputs necessary and technical properties for the GT cycle.

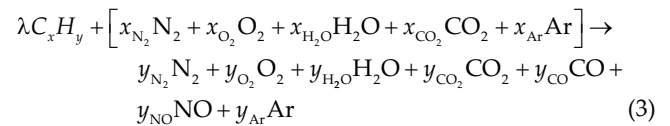
GT simulation has been presented in many other papers [23–30]. So, in this section, the differences, as compared to other models, are presented. Compressor inlet pressure is given by Eq. (1).

$$P_{atm} = \frac{(760 \times (1 - 226 \times 10^{-7} \times H)^{5.25})}{735} \tag{1}$$

where  $H$  is the altitude and  $P_{atm}$  is written in the bar unit. Air moisture is also introduced to this simulation, and this parameter effects the molar fraction of water. The amount of cold pressure reduction, which is presented in [24], and hot pressure reduction are both considered in GT [24].

$$\Delta P_{hot} = 0.5\rho U^2 \left( \frac{T_c}{T_b} \right) - 1 \tag{2}$$

Major pressure reduction, which takes place in the combustion chamber, results from the combustion process itself. It is dependent on the output velocity from a compressor ( $U$ ) (m/s), the inlet and outlet air temperature ( $T_b, T_c$ ) (K) of the combustion chamber, and the density of the inlet air ( $\rho$ ) ( $kg/m^3$ ). Combustion equation, percentage of the contribution of each component and energy equation are presented in Eqs. (3)–(10), respectively.



$$y_{CO_2} = \lambda x + x_{CO_2} - y_{CO} \tag{4}$$

$$y_{H_2O} = \frac{\lambda y}{2} + x_{CO_2} \tag{5}$$

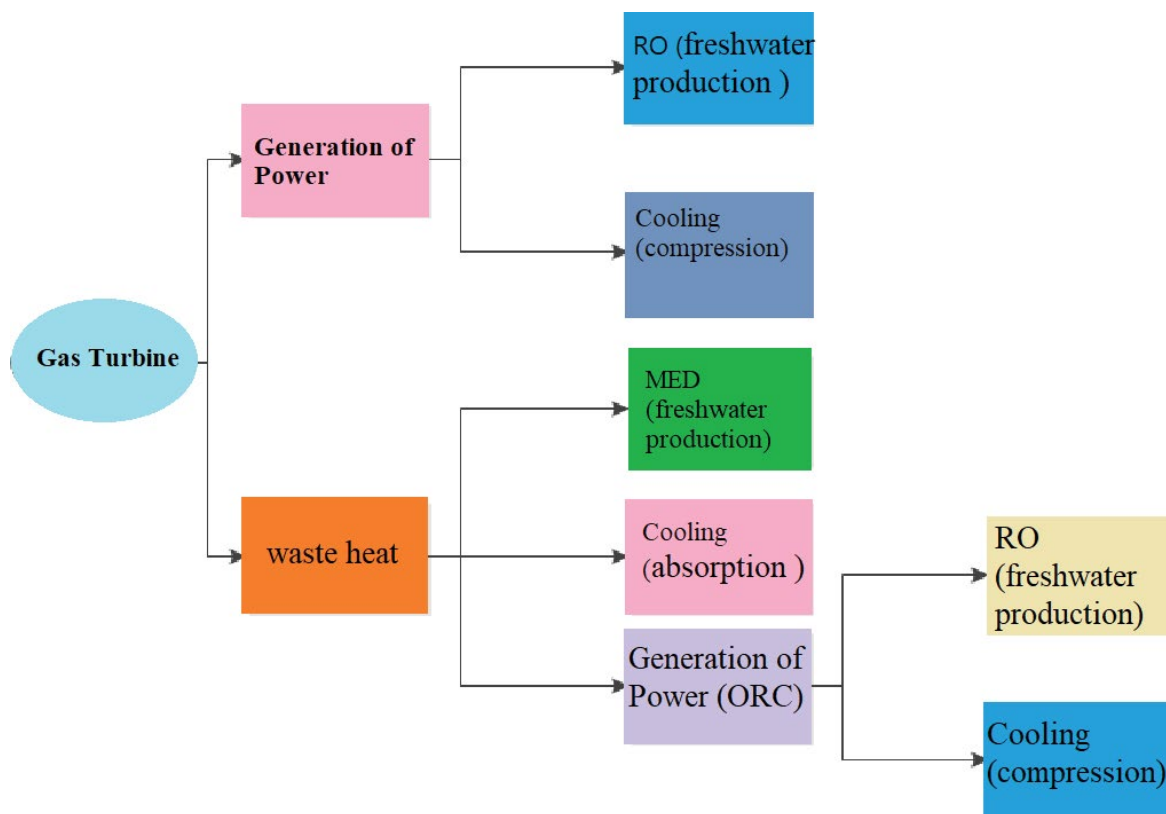


Fig. 2. Flowchart for the various cycles of the studied combined system.

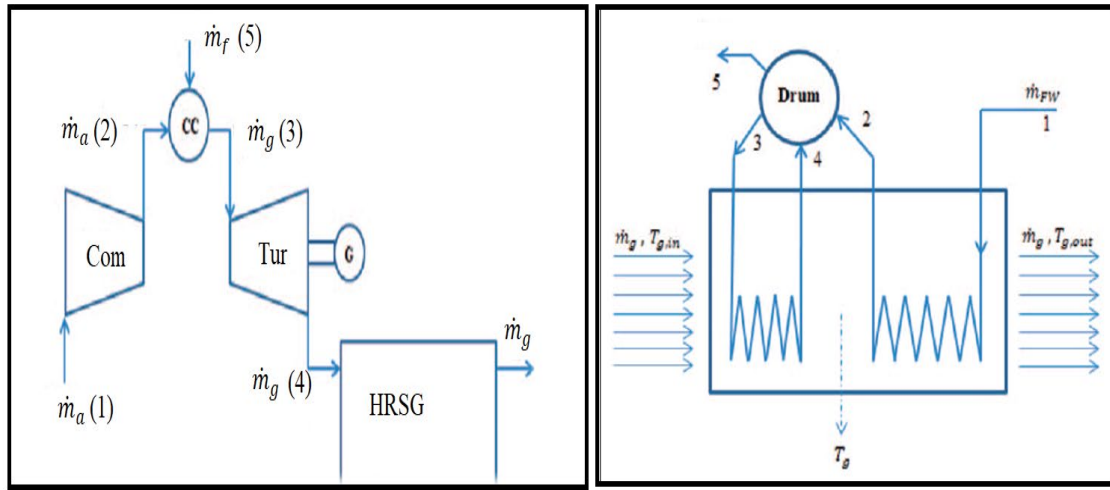


Fig. 3. Schematic of the combined gas turbine and HRSG system.

Table 1  
Input parameters and technical properties for the GT system

Parameter	Value
Compressor pressure ratio	5.3
Fuel type	Natural gas
Gas turbine inlet temperature (TIT) (100 %load), °C	850
Compressors isentropic efficiency, %	85.5
Isentropic gas turbine efficiency, %	86
Annual average ambient temperature, °C	28
Annual average humidity, %	75
Altitude, m	1/25
Fuel lower heating value, MJ/kg	46.25
Power generation, MW	9.53
Exhaust temperature, °C	514.8
Exhaust gas flow, kg/s	44.87
Efficiency, %	28.8

$$y_{Ar} = x_{Ar} \quad (6)$$

$$y_{N_2} = x_{N_2} - \frac{y_{Co}}{2} \quad (7)$$

$$y_{O_2} = x_{O_2} + \frac{y_{Co} y_{No}}{2} - \lambda x - \frac{\lambda y}{4} \quad (8)$$

$$\bar{h}_{air} + \lambda \bar{h}_{fuel,inlet} = (\bar{h}_{gas} (1 + \lambda))_{product} + (0.02 \times LHV + \bar{\lambda}) \dot{Q}_{loss} \quad (9)$$

$$\bar{\lambda} = \frac{X_{O_2} \Delta \bar{h}_{O_2} + X_{N_2} \Delta \bar{h}_{N_2} + X_{CO_2} \Delta \bar{h}_{CO_2} + X_{H_2O} (\bar{h}_{H_2O, T_D} - \bar{h}_{H_2O, T_C})}{\bar{h}_f + X \bar{h}_{O_2, T_D} - \frac{Y \bar{h}_{O_2, T_D}}{4} - X \bar{h}_{CO_2, T_D} + \frac{Y \bar{h}_{H_2O, T_D}}{2} - 0.02 \times LHV} \quad (10)$$

where  $\lambda$  is defined as the molar fuel to air ratio, as written in Eq. (11):

$$\bar{\lambda} = \frac{\dot{m}_f}{\dot{m}_{air} \times \frac{M_{air}}{M_f}} \quad (11)$$

In Eq. (3), “ $x$ ” and “ $y$ ” are the amounts of carbon and hydrogen in the fuel, which can be calculated based on the fuel being used in the power plant. Eqs. (4)–(8) are derived from the balance of components. As the enthalpy of combustion products and air is determined by  $\bar{h} = \sum_{i=1}^N X_i \bar{h}_i$ , then Eq. (10) can be written by merging this equation in Eq. (9). GT simulation is expressed as in [24,31]. In the current simulation, the power reduction is induced by HRSG on the GT, which can be the result of the gas side pressure reduction, as considered and written in [24,27,30]:

$$\Delta W = \dot{m}_g C_{p_g} \eta_t T_{i,GT} \left[ \left( \frac{P_{atm}}{P_{i,GT}} \right)^{\frac{\gamma-1}{\gamma}} - \left( \frac{P_{atm} + DP_g}{P_{i,GT}} \right)^{\frac{\gamma-1}{\gamma}} \right]; \gamma = \frac{C_{p_g}}{C_{p_g} - 1} \quad (12)$$

In Eq. (12),  $DP_g$  is the gas side pressure reduction in HRSG,  $\eta_t$  is the turbine efficiency,  $T_{i,GT}$  is the GT input temperature, and  $C_{p_g}$  is the specific heat capacity of the gas.

### 2.2.2. Heat recovery boiler design

According to Fig. 3, the first step is to solve the energy equations. Thermodynamic parameters can be calculated by writing energy equations for the economizer [Eq. (13)], the evaporator [Eq. (14)], the superheater [Eq. (15)], and the auxiliary approach ( $T_{ap}$ ) and pinch ( $T_{pinch}$ ) equations [Eqs. (16) and (17), respectively]. These equations are expressed as follows [24,27,32]; they can be calculated by solving a set of equations for each level of pressure [27]:

$$\dot{m}_g C_{p_g} (T_{g,o} - T_{g,i}) = \dot{m}_{feed} C_{p_g} (h_{w,o} - h_{w,i}) \quad (13)$$

$$\dot{m}_g C_p (T_{g,o} - T_{g,i}) = \dot{m}_{feed} [(h_v - h_{w,o}) + BD(h_l - h_{w,o})] \quad (14)$$

$$\dot{m}_g C_p (T_{g,o} - T_{g,i}) = \dot{m}_{feed} (h_{s,o} - h_{s,i}) \quad (15)$$

$$T_{ap} = (T_{sat} - T_{w,o}) \quad (16)$$

$$T_{pinch} = (T_{g,o,eva} - T_{sat}) \quad (17)$$

where  $\dot{m}_g$  is the gas mass flow rate (kg/s),  $T_{g,i}$ ,  $T_{sat}$  and  $T_{w,o}$  are the input gas, saturated water, and output water temperature (°C),  $h_v$ ,  $h_l$ ,  $h_{w,o}$  and  $h_s$  are liquid, water output, vapor and superheat enthalpy (kJ/kg), respectively, and BD is the blow-down. The second step is to calculate the thermal areas. To design the HRSG system, it is essential to calculate the heat transfer areas, which can be obtained by [30]:

$$A = \frac{\dot{Q}}{U \Delta T_{LMTD}} \quad (18)$$

where  $\dot{Q}$  and  $\Delta T_{LMTD}$  are the heat flow rate and the logarithmic temperature difference. The logarithmic mean temperature difference and the overall heat transfer coefficient can be determined as follows:

$$\Delta T_{LMTD} = F_T \times \frac{\Delta T_{max} - \Delta T_{min}}{\ln \left( \frac{\Delta T_{max}}{\Delta T_{min}} \right)} \quad (19)$$

$$\frac{1}{U} = \frac{1}{\eta_o h_o} + f_o + \frac{A_t}{A_{wi}} f_i + \frac{A_t}{A_{wi}} \frac{1}{h_i} + \frac{A_t}{A_w} \frac{d_o \ln \left( \frac{d_o}{d_i} \right)}{2K_m} \quad (20)$$

where  $F_T$  is a coefficient representing the angle of incidence between the gas flow and pipes [27].

In this research, “U” was assumed to be in the range of 20–50 (W/m<sup>2</sup> K) for the economizer and in the range of 70–110 (W/m<sup>2</sup> K) for the evaporator. Therefore, U was considered as the average value of this range, which was 35

(W/m<sup>2</sup> K) for the economizer and 90 (W/m<sup>2</sup> K) for the evaporator [27].

### 2.2.3. ORC system modeling

ORC system modeling was also performed based on the continuity law and the first law of thermodynamics. According to Fig. 1, the schematics of a basic cycle of the ORC system is shown in Fig. 4. As can be observed in Fig. 4, there are four different processes: process 1–2 (pumping process), process 2–3 (constant pressure heat addition), process 3–4 (expansion process), and process 4–1 (constant pressure heat removal). Table 2 consists of the inputs necessary and the technical properties for the ORC cycle.

The equations used to evaluate the ORC system are presented in Table 3 [33].

The important point in the ORC system is to determine the appropriate working fluid based on temperature conditions. Fig. 5 shows the algorithm used to determine the optimal working fluid [34]. The intended fluids were selected based on the critical temperature conditions as well as the environmental impacts of the ORC fluid.

According to Table 4, which is proportional to the heat source temperature, the fluids and the role of environmental factors were investigated in this study.

### 2.2.4. RO system modeling

According to Fig. 1, the schematics of the RO system is shown in Fig. 6. By considering the mass transfer relations, in RO system modeling, it can be found that the intensity of the flow of water and salt passing the membrane is in the form of the relations (26) and (27). Additionally, the mean velocity in each element of the membrane is determined in the relation (28). The concentration of salt in the produced water is determined by the relation (29). Moreover, due to the polarization phenomenon, the concentration of the mass transfer process of salt concentration near the wall is calculated based on the theory of film, as represented in Eq. (30). By considering the continuity equation, one can use Eqs. (31) and (32) for the diffusion flow and saline water flow, respectively [35,36]:

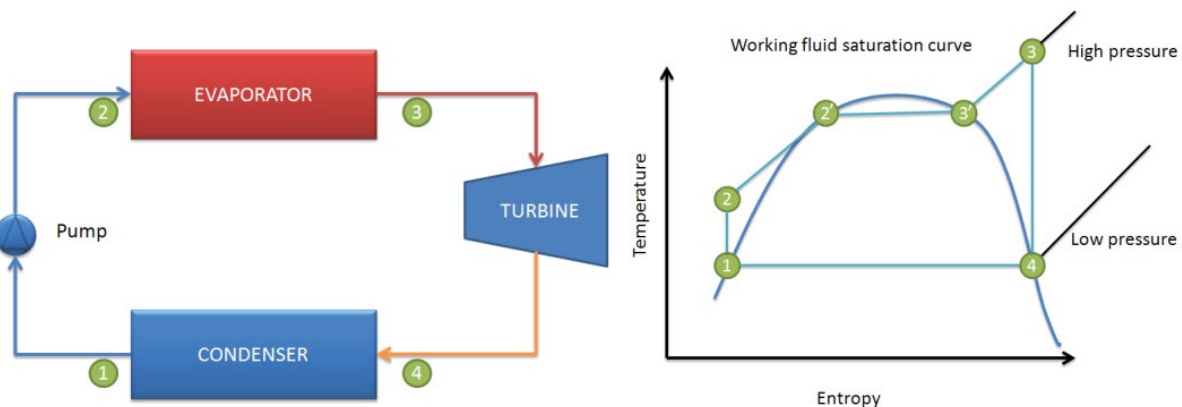


Fig. 4. Schematic diagram of the ORC system with the T-S diagram.

Table 2  
Input parameters and technical properties for the ORC system

Parameter	Value
$T_{pinch}$ , °C	20
$T_{app}$ , °C	5
Turbine inlet pressure, bar	25
Efficiency, %	16.6

Table 3  
Thermodynamic equations used to evaluate the ORC system

Component	Equation
Pump (1–2)	$\dot{W}_p = \frac{\dot{W}_{p,ideal}}{\eta_p} = \frac{\dot{m}(h_1 - h_{2s})}{\eta_p}$ (21)
Evaporator (2–3)	$\dot{Q}_e = \dot{m}(h_3 + h_2)$ (22)
Turbine (3–4)	$\dot{W}_t = \frac{\dot{W}_{t,ideal}}{\eta_t} = \frac{\dot{m}(h_3 - h_{4s})}{\eta_t}$ (23)
Condenser (4–1)	$\dot{Q}_c = \dot{m}(h_1 - h_4)$ (24)
Cycle efficiency	$\eta_{cycle} = \frac{\dot{W}_t + \dot{W}_p}{\dot{Q}_e}$ (25)

$$J_w = A \times TCF \left[ \left( P_f - P_p - \frac{\Delta P_f}{2} \right) - (\pi_w - \pi_p) \right] \times 10^6 \quad (26)$$

$$J_s = B(C_w - C_p) \quad (27)$$

$$V_w = \left( \frac{J_w + J_s}{\rho_p} \right) \quad (28)$$

$$C_p = \frac{J_s}{V_w} \times 1,000 \quad (29)$$

$$C_w = C_p + \left( \frac{C_f + C_b}{2} - C_p \right) e^{V_w/k} \quad (30)$$

$$Q_p = V_w \times S_m \quad (31)$$

$$Q_B = Q_f \times Q_p \quad (32)$$

$$C_B = \frac{Q_f C_f - Q_p C_p}{Q_B} \quad (33)$$

In these equations,  $A$  is the water permeability coefficient [ $\text{kg}/\text{m}^2 \text{ s Pa}$ ],  $B$  is the solute transport coefficient [ $\text{kg}/\text{m}^2 \text{ s}$ ],

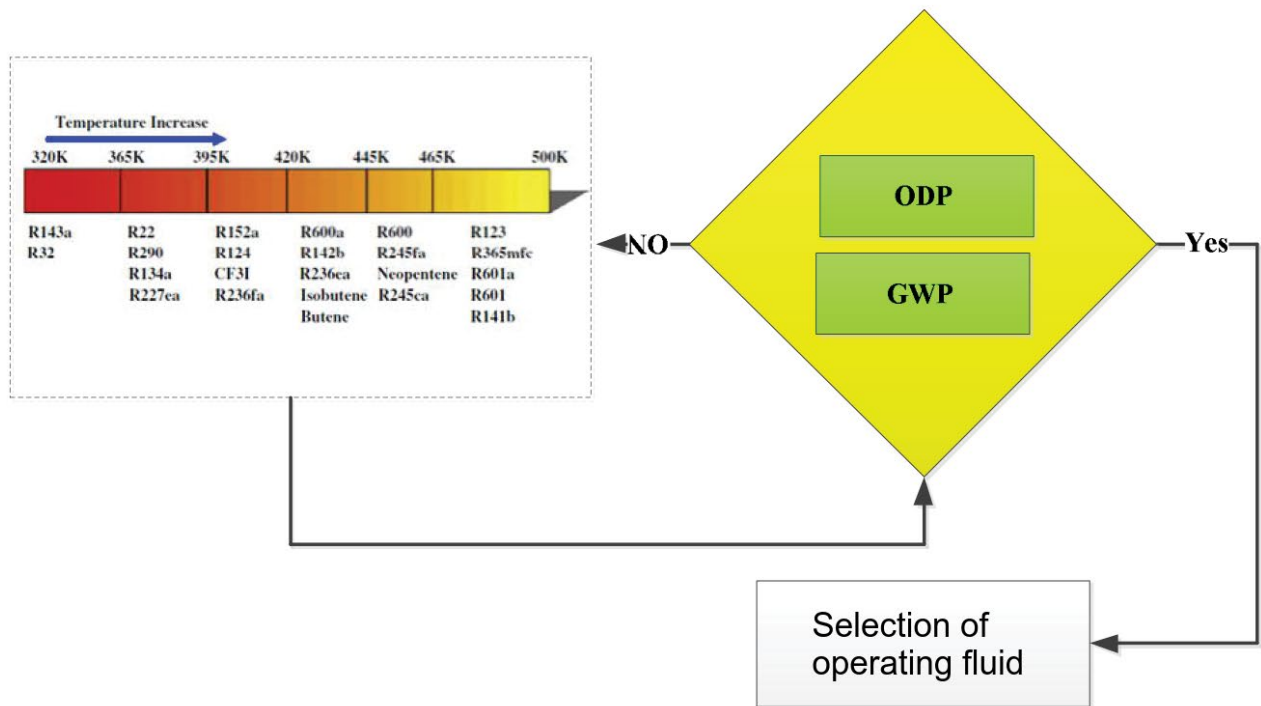


Fig. 5. The algorithm used to determine the working fluid of the ORC system based on the critical temperature.

Table 4  
Characteristics of the investigated fluids in the simple ORC

Number	Fluid	Boiling temperature at 1 bar (K)	Critical pressure (Mpa)	Critical temperature (K)
1	n-Butane	272.6	3.8	425.13
2	R245fa	288.05	3.6	427.2
3	R245ca	298.28	3.9	447.57
4	R123	300.97	3.7	456.83
5	R141b	305.2	4.5	479.96

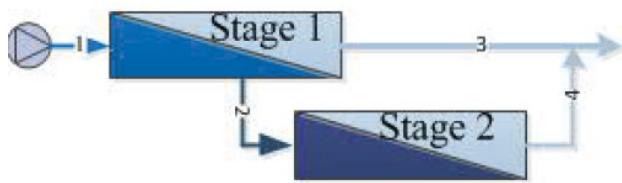


Fig. 6. Schematic of the RO system.

$C_f$  is the brine concentration at the membrane feed side surface [kg/m<sup>3</sup>],  $\pi$  is the local osmotic pressure of the solutions [MPa],  $J_w$  refers to the local permeate flux [kg/m<sup>2</sup> s],  $J_s$  represents the local solute flux [kg/m<sup>2</sup> s],  $V_w$  is the permeate velocity [m/s],  $\rho_p$  is the density of the permeate [kg/m<sup>3</sup>],  $Q$  is the flow rate [m<sup>3</sup>/h], and  $C$  is concentration [ppm] (subscripts: *b*: brine stream, *f*: feed stream, *p*: permeate stream, and *w*: membrane wall). Relations that can be used to reduce the number of unknowns are as follows [35,37]:

$$k = 0.04 \times \text{Re}^{0.75} \times \text{Sc}^{0.33} \times \left( \frac{D_s}{d} \right) \quad (34)$$

$$\Delta P_f = \frac{0.0033 Q_a L_{PV} \mu}{W d^3} \quad (35)$$

$$\pi = \frac{0.2641 \times C (T + 273) \mu}{10^6 - C} \quad (36)$$

where Re (Reynolds number) is  $\rho V_w d / \mu$ ,  $K$  is the local mass transfer coefficient (m/s),  $\mu$  is the liquid viscosity (Pa s),  $D_s$  is the solute diffusivity (m<sup>2</sup>/S),  $d$  is the feed channel equivalent diameter, and  $Q_a \left( \frac{Q_b + Q_f}{2} \right)$  is the mean discharge. Also,

$L_m$  is the membrane length and  $N$  is the number of elements in each pressure vessel (PV). To add,  $\pi$  is the osmotic pressure and  $C$  is the salt concentration. To estimate the mean of the pressure loss, the Hagen–Poiseuille equation was used. Schmidt number ( $\text{Sc} = \mu / \rho D_s$ ) was calculated according to the Eqs. (9) and (10). Concentration polarization could be calculated using the Sc number. For one spiral wound membrane element, each of the feed water and product flows could be considered as the flow between two parallel plates with a length of  $L$ , a width of  $W$ , and the distance of  $d$ ; according to it, the pressure drop on the feed side can be

calculated. For a spiral wound element, the membrane width of  $W$  can be calculated using the relation  $S_m = W \times L \times N_p$ ; based on the membrane area and the number of plates ( $N_p$ ), Table 5 represents the inputs necessary for the RO system.

### 2.2.5. Multi-effect water desalination system modeling

According to Fig. 1, the schematics of the MED system is shown in Fig. 7. In designing the MED system, relations are divided into three general groups: the first group includes the relations related to the continuity equations and the produced water discharge; the second group consists of the equations related to energy, and the third one represents the equations related to the area required for heat transfer and heat transfer coefficients, as shown in Tables 6–8, respectively.

In these equations,  $A$  is the heat transfer surface (m<sup>2</sup>),  $B$  is the brine density (kg/s),  $C$  is the concentration (ppm),  $D$  is the freshwater discharge (kg/s),  $F$  is the feedwater mass flow rate (kg/s),  $Q$  is the produced water flow rate (m<sup>3</sup>/d),  $S$  is the injection vapor pressure (kg/s),  $T$  is the temperature in °C,  $L$  is the latent heat of vaporization,  $y$  is the flashed fraction, and  $n$  is the number of effects.

Data for the MED simulation included: pipe length: 4.1 m, steam pressure: 8.5 bar and input feed water temperature: 25°C.

Table 5  
Input parameters for RO modeling

Parameter	Value
Feed water flow, m <sup>3</sup> /h	80
Input feed water temperature, °C	25
Environment pressure, bar	1
PV number	3
Number of membranes per PV	6
Membrane type	BW30-400 (spiral wound)
Pure water permeability constant, (kg/m <sup>2</sup> s Pa)	$7.5 \times 10^{-9}$
Salt permeability constant, (kg/m <sup>2</sup> s)	$6.2 \times 10^{-5}$
Outer radius of the fiber bundle, m	$201 \times 10^{-3}$
Inner radius of the fiber bundle, m	$29 \times 10^{-3}$
Length of fiber bundle, m	$1,016 \times 10^{-3}$
Feed space, m	$863.6 \times 10^{-6}$
System stage number	2
Recovery, %	75

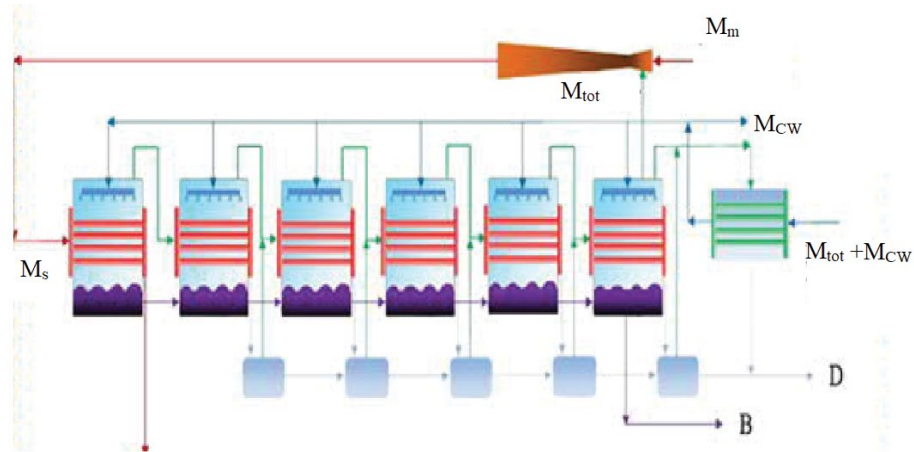


Fig. 7. Schematics of the MED system.

Table 6  
Mass balance equations, GOR and freshwater production [6,38]

Equations	Description	
$B_1 = F_1 - D_1$	Mass balance in the first effect	(37)
$B_i = F_i + B_{i-1} - D_i + \left[ y_{i-1} \left( D_r + \sum_{j=1}^{i-2} D_j \right) \right] - [(i-1)F_{i-1}y_{i-1}]$	Mass balance from the second effect to $n^{\text{th}}$ effect	(38)
$D_{\text{con}} = D_n - D_r + \left[ y_n \left( D_r + \sum_{i=1}^{n-1} D_i \right) \right]$	Mass balance in the condenser	(39)
$D = \left[ (1 - y_n) \left( D_r + \sum_{i=1}^{n-1} D_i \right) \right] - \left[ y_{n-1} \left( D_r + \sum_{i=1}^{n-2} D_i \right) \right] - \left[ y_{n-2} \left( D_r + \sum_{i=1}^{n-3} D_i \right) \right] - \left[ y_{n-3} \left( D_r + \sum_{i=1}^{n-4} D_i \right) \right] - \left[ y_{n-4} \left( D_r + \sum_{i=1}^{n-5} D_i \right) \right] - (y_{n-5} \times D_r) + D_{\text{con}} \times y_6$	Mass balance in distillation tank	(40)
$C_{\text{sw}} F_1 = C_{B_1} B_1$	Salt balance in the first effect	(41)
$C_{\text{sw}} F_i + (C_{B_{i-1}} B_{i-1}) = C_{B_i} B_i$	Salt balance from the second effect to $n^{\text{th}}$ effect	(42)
$\text{GOR} = \frac{D}{S}$	Maximum rate of available output	(43)

Table 7  
Energy balance equations [38]

Equations	Description	
$D_1 L_1 + (F_1 C_p (T_1 - T_{f1})) = (D_r + S) L_0$	Energy balance in the first effect	(44)
$D_i L_i + (F_i C_p (T_i - T_{fi})) = (D_{i-1} L_{i-1}) + \left( y_{i-1} \left( D_r + \sum_{j=1}^{i-2} D_j \right) L_{i-1} \right) - (i-1)(F_{i-1} y_{i-1} L_{i-1}) + (B_{i-1} C (T_{i-1} - T_i))$	Energy balance from the second effect to $n^{\text{th}}$ effect	(45)

Table 8  
Equations for calculating heat surfaces and heat transfer coefficients [38]

Equations	Description
$A_{e1} = \frac{(D_r + S)L_0}{U_{e1} \times (T_{0c} - T_1)}$	First effect surface (46)
$A_{ej} = \frac{\left( \left( y_{i-1} \left( D_r + \sum_{i=1}^{i-2} D_i \right) + D_{i-1} \right) - (i-1)(F_i Y_{i-1}) \right) L_{i-1}}{U_{ej} \times (T_{vi-1} - T_i)}$	Second effect surface and next effects surfaces (47)
$A_{Hi} = \frac{(i \cdot F_i \cdot C \cdot (T_{fi} - T_{fi+1}))}{U_{Hi} \cdot \text{LMTD}_{Hi}}$	First to $n-1$ preheater surface (48)
$A_{Hn} = \frac{(n \cdot F_n \cdot C \cdot (T_{fn} - T_f))}{U_{Hn} \cdot \text{LMTD}_{Hn}}$	$n^{\text{th}}$ preheater surface (49)
$A_{\text{con}} = \frac{\left( y_n \left( D_r + \sum_{i=1}^{n-1} D_i \right) + D_{\text{con}} \right) - (i-1)(F_i y_{i-1}) L_n}{U_{\text{con}} \cdot \text{LMTD}_{\text{con}}}$	Condenser heat transfer surface (50)
$U_{e1} = 1.9394 + (1.40562 \times 10^{-3})T_{0c} - (2.07525 \times 10^{-5})T_{0c}^2 + (2.3186 \times 10^{-6})T_{0c}^3$	Heat transfer coefficient of the first effect (51)
$U_{ei} = 1.9394 + (1.40562 \times 10^{-3})T_{vi-1} - (2.07525 \times 10^{-5})T_{vi-1}^2 + (2.3186 \times 10^{-6})T_{vi-1}^3$	Heat transfer coefficient of the second to $n^{\text{th}}$ effect (52)
$U_{Hi} = 14.1825162 + (0.011381865)T_{vi} + 0.013381501T_{fi+1}$	Preheater transfer coefficient to $n-2$ (53)
$U_{Hn-1} = 14.1825162 + (0.011381865)T_{vn-1} + 0.013381501T_f$	Preheater transfer coefficient to $n-1$ (54)
$U_{\text{con}} = 1.6175 + (1.537 \times 10^{-4})T_{vn} - (1.825 \times 10^{-4})T_{vn}^2 + (8.026 \times 10^{-8})T_{v0}^3$	Condenser heat transfer coefficient (55)

2.2.6. Cooling systems modeling

The compression refrigeration system modeling was performed based on the first law of thermodynamics; According to Fig. 1, the thermodynamics of the vapor compression cycle can be analyzed on a temperature vs. entropy diagram, as depicted in Fig. 8.

Table 9 consists of the inputs necessary for the compression refrigeration system.

Theoretical analysis of vapor compression cooling [39]:

From stage 1 to stage 2, work is put into the compressor; thus,

$$\dot{W}_{\text{comp}} = \dot{m}(h_2 - h_1) \tag{56}$$

From stage 2 to stage 3, heat is given off through the condenser; thus,

$$\dot{Q}_{\text{cond}} = \dot{m}(h_2 - h_3) \tag{57}$$

From stage 3 to stage 4, the enthalpy of the refrigerant stays approximately constant; thus,

$$h_3 = h_4 = h \quad (x=0, P=P_3) \tag{58}$$

From stage 1 to stage 4, heat is put into the system; thus,

$$\dot{Q}_{\text{evap}} = \dot{m}(h_2 - h_4) \tag{59}$$

where

$$h_1 = h_{\text{sat}}(P = P_1) \tag{60}$$

$$\dot{Q}_{\text{cond}} = \dot{Q}_{\text{evap}} + \dot{W}_{\text{comp}} \tag{61}$$

The coefficient of performance describes the efficiency of the evaporator in absorbing heat in relation to the work put in; thus,

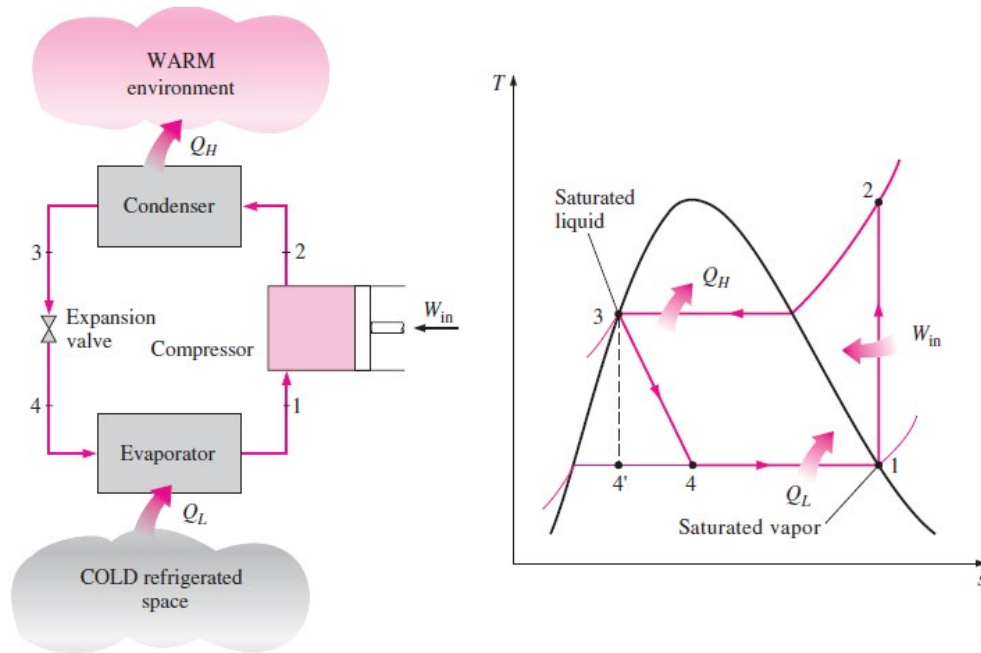


Fig. 8. Schematic diagram of the compression refrigeration system with the T-S diagram.

Table 9  
Input parameters for modeling the compression refrigeration system

Parameter	Value
Compressor efficiency, %	80
Evaporator pressure, kPa	200
Condenser pressure, kPa	500

$$COP = \frac{\dot{Q}_{evap}}{\dot{W}_{comp}} \tag{62}$$

Additionally, single-effect LiBr-H<sub>2</sub>O absorption system modeling was performed based on the study [39,40]. According to Fig. 1, the schematics of a single-effect absorption refrigeration system is shown in Fig. 9.

Table 10 consists of the inputs necessary for the single-effect absorption refrigeration system.

The performance of the absorption chiller is determined by its cooling capacity, the generator heat input, and coefficient of performance (COP). These quantities could be defined by the following equations. The cooling capacity or chiller load can be calculated as [40]:

$$\dot{Q}_{evap} = \dot{m}_{ch} (h_{ch,i} - h_{ch,o}) \tag{63}$$

$$\dot{Q}_{evap} = \dot{Q}_{load} \tag{64}$$

$$\dot{m} = \frac{\dot{Q}_{load}}{h_{ch,i} - h_{ch,o}} \tag{65}$$

The heat supplied to the generator is:

$$\dot{M}_{weak} = \frac{x_4 - x_7}{x_4 - x_3} \times \dot{m} \tag{66}$$

$$\dot{Q}_G = \dot{m}_{ge} (h_{ge,i} - h_{ge,o}) \tag{67}$$

Finally, the instantaneous COP of the chiller can be determined as:

$$(COP)_{actual} = \frac{\dot{q}_{eva}}{\dot{q}_{gen}} \tag{68}$$

### 2.2.7. Economic modeling

In addition, to considering technical investigations and thermodynamic constraints, economic analysis should also be taken into account in the determination and selection of a design. The total annual cost (TAC) consists of two terms including operating costs (OC) and the total capacity investment (TCI). TCI includes fixed capital investment (FCI), startup costs (SUC), working costs (WC), license obtaining fees and research and development cost (LRD), and the cost of the estimated lack of budget during construction (AFUDC) (relation 69) [31]:

$$TCI = FCI + SUC + WC + LRD + AFUDC \tag{69}$$

where FCI includes direct costs (DC) and indirect costs (IC); it can be supposed that IC is 0.25 times more than DC. The design DC can be calculated using Eq. (70), including onsite costs (ONSC) and offsite costs (OFSC) [31]:

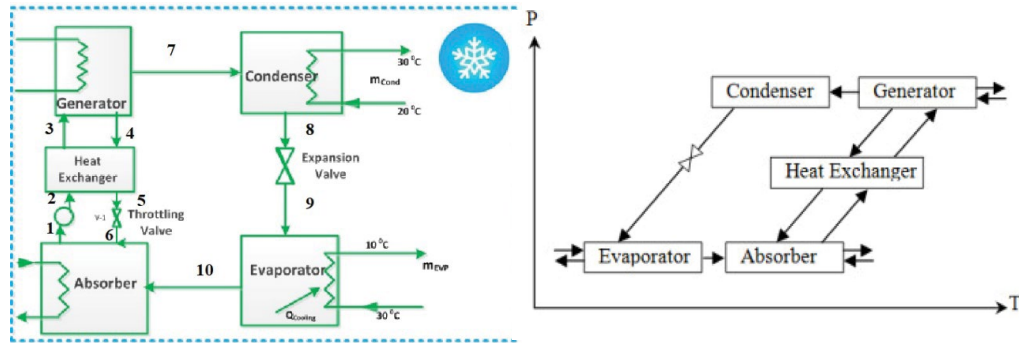


Fig. 9. Schematic diagram of the single-effect LiBr-H<sub>2</sub>O absorption refrigeration system with the P-T diagram.

Table 10  
Input parameters for modeling the single-effect absorption refrigeration system

Parameter	Value
$T_{cod} = T_{abs}$ , °C	37.8
$T_{gen}$ , °C	87.8
$T_{eva}$ , °C	7.2

$$DC = ONSC + OFSC \quad (70)$$

$$OFSC = \begin{cases} 1.2 \times ONSC & \text{new system} \\ 0.45 \times ONSC & \text{expansion} \end{cases} \quad (71)$$

$$WC = 0.15 \times TCI \quad (72)$$

$$SUC = 0.1 \times TCI \quad (73)$$

Research and development cost and IC can be calculated as follows [31]:

$$LRD = AFUDC + 0.15 \times FCI \quad (74)$$

The value of TCI can be calculated using the relation (75):

$$TCI = 1.47 \times FCI \quad (75)$$

As a result:

$$TCI = 1.84 \times DC = 1.84 \times (ONSC + OFSC) \quad (76)$$

TCI can also be calculated by combining the above-mentioned relations and using relation (77):

$$TCI = \begin{cases} 4.05 \text{ ONSC} & \text{new system} \\ 2.67 \text{ ONSC} & \text{expansion} \end{cases} \quad (77)$$

Experience has shown that the cost of fixed investment in a new system is between 2.8 and 5.5 times more than that of purchasing equipment [31]; therefore:

$$FCI = \begin{cases} 2.8 - 5.5 \text{ CC} & \text{new system} \\ 2.83 \text{ CC} & \text{expansion} \end{cases} \quad (78)$$

By combining relations, the relation (79) is obtained:

$$TCI = \begin{cases} 4.12 - 8.09 \text{ CC} & \text{new system} \\ 4.16 \text{ CC} & \text{expansion} \end{cases} \quad (79)$$

Table 11  
Cost of the RO system components [35]

Equation	Component
$CC_{swip} = 996(Q_f 24)^{0.8}$	Capital cost of the seawater intake and pre-treatment (80)
$CC_{hpp} = 52(Q_{hpp} \Delta P_f)$	Capital cost of high-pressure pump and pre-treatment (81)
$CC_{bp} = a_1 (mV \Delta P)^{a_3} f_m \phi_\eta$ $\phi_\eta = 1 + \left( \frac{1 - \bar{\eta}_1}{1 - \eta_1} \right)^{a_3}$ & $f_m = \begin{cases} \text{Cast iron} = 1 \\ \text{Steel} = 1.41 \end{cases}$	Pump cost (82)
$f_m$ : materials correction factor, $f_m = 1.41$ , $\phi_\eta$ : first law efficiency correction factor, $a_1 = 549.13 \frac{\$}{\text{Kw}^{0.71}}$ , $a_2 = 0.71$ , $a_3 = 3$ , $\bar{\eta}_1 = 0.8$	
$CC_m = \sum_{j=1}^{N_{RO}} C_k n_{m,j} n_{pv,j} + \sum_{j=1}^{N_{RO}} C_{pv} n_{pv,j}$	Total membrane module cost (83)

Table 12  
MED purchase cost [38]

Equations	Description	
$C_A = 140 \times A_{E\&C}$	Area costs (\$)	(84)
$C_{\text{equipment}} = 4 \times C_A$	Instrument cost (evaporator, condenser...) (\$)	(85)
$C_{\text{site}} = 0.2 \times C_{\text{eq}}$	Site cost (\$)	(86)
$C_{\text{tr}} = 0.05 \times (C_A + C_{\text{eq}} + C_s)$	Transportation costs (\$)	(87)
$C_b = 0.15 \times C_{\text{eq}}$	Building construction cost (\$)	(88)
$C_{\text{en}} = 0.1 \times C_{\text{eq}}$	Engineers and salary costs (\$)	(89)
$C_c = 0.1 \times (C_A + C_{\text{eq}} + C_s)$	Contingency costs (\$)	(90)
$CC_{\text{MED}} = C_A + C_{\text{equipment}} + C_{\text{site}} + C_{\text{tr}} + C_b + C_{\text{en}} + C_c$	Capital costs (\$)	(91)

With having the cost of purchasing equipment (CC) and ONSC, TCI can be estimated. Equations are used to estimate the cost of each component of the RO system, as shown in Table 11. Table 12 shows the costs of MED. It is worth mentioning that the cost of HRSG is obtained from [23,31].

Additionally, the price of purchasing ORC and cooling equipment is presented in Appendix A.

In these relations,  $A_{E\&C}$  is the sum of the area of the condenser and effects. The RO system operation cost is calculated as follows [35]:

$$OC_m = 0.2 \times CC_m \quad (92)$$

$$OC_{\text{inserece}} = 0.005 \times \text{TCI} \quad (93)$$

$$OC_{\text{labor}} = Q_p \times 24 \times 365 \times f_c \times 0.01 \quad (94)$$

$$OC_{\text{main}} = Q_p \times 24 \times 365 \times f_c \times 0.01 \quad (95)$$

$$OC_{\text{ch}} = Q_p \times 24 \times 365 \times f_c \times 0.0225 \quad (96)$$

$$OC_{O\&M,RO} = OC_{\text{inserece}} + OC_{\text{labor}} + OC_{\text{ch}} + OC_{\text{main}} \quad (97)$$

$$AOC_{RO} = OC_m + OC_{O\&M,RO} \quad (98)$$

In these equations,  $OC_m$  is the cost of replacement.  $OC_{O\&M}$  is the sum of the operation cost, including  $OC_{\text{labor}}$ ,  $OC_{\text{main}}$ ,  $OC_{\text{ch}}$  and  $OC_{\text{inserece}}$ , which are the annual costs of laboratory, the annual maintenance costs, the annual cost of chemicals and the insurance cost, respectively. The operation cost of the MED system is calculated as follows [35]:

$$C_{\text{el}} = c_{\text{el}} \times P \times f_c \times Q_p \times 365 \quad (99)$$

$$C_l = 0.1 \times f_c \times Q_p \times 365 \quad (100)$$

$$C_{\text{ch}} = 0.04 \times f_c \times Q_p \times 365 \quad (101)$$

$$C_{\text{in}} = 0.005 \times C_A \quad (102)$$

$$AOC_{\text{MED}} = C_{\text{th}} + C_{\text{el}} + C_l + C_{\text{ch}} + C_{\text{in}} \quad (103)$$

where  $C_{\text{el}}$  is the electricity cost,  $C_l$  is the laboratory cost,  $C_{\text{ch}}$  is the chemicals cost,  $C_{\text{in}}$  is insurance costs and finally,  $AOC_{\text{MED}}$  is the annual operation costs. Also, the sum of annual operation costs is calculated as follows:

$$AOC_{\text{Total}} = AOC_{\text{Other}} + AOC_{\text{RO or MED}} \quad (104)$$

The TAC is given by Eq (105):

$$\text{TAC} = \frac{\text{TCI}}{\text{CRF}} + AOC_{\text{Total}} \quad (105)$$

Capital recovery factor (CRF) depends on the interest rate and the estimated life of the equipment, which can be determined using Eq. (106):

$$\text{CRF} = \frac{i(1+i)^{\text{year}}}{(1+i)^{\text{year}} - 1} \quad (106)$$

where the year is the design useful life and  $i$  is the interest rate, which has been considered the same for both water desalination systems. Finally, the amount of the freshwater unit production cost (UPC) is calculated as follows [35]:

$$\text{UPC} = \frac{\text{TAC}}{24 \times Q_p \times 365} \quad (107)$$

In this economic modeling, the input parameters are considered according to Table 13.

### 3. Results and discussion

#### 3.1. Validation

Given that the intended cycle has been composed of several parts, the validation of the present study in its three important sections is presented.

##### 3.1.1. ORC section

The organic fluid properties were extracted based on the Refprop software. Validation of the Rankine organic cycle section using [33] was performed for each cycle. The results of this investigation are shown in Table 14. As could be observed, the error in this section was acceptable.

##### 3.1.2. RO system section

Based on the membranes produced, each company has developed some software included by default in the software database of its membrane data. In this part, the code developed by MATLAB software was validated using the DOW company software with the commercial name of ROSA. The flow rate and the concentration of the feed water were considered to be 80 m<sup>3</sup>/h and 4,049 TDS, respectively. In the feed water, only salt (NaCl) was considered. According to Table 15, the maximum error percentage was equal to 14%.

##### 3.1.3. MED system section

Results from the MED validation can be seen in Table 16.

#### 3.2. Results

Fig. 10 shows gas turbine power and ORC variations in terms of changes at the ambient air temperature. As the ambient air temperature was increased, the gas turbine produced work was decreased due to the reduction of the air mass flow rate and the increase of the compressor power. The output power changes in ORC with R123 fluid, with ambient air temperature changes and the mass flow rate of exhaust gas from the gas turbine, are also shown in this figure. As shown, by increasing the mass flow rate of the exhaust gas from the gas turbine (i.e., ambient air

temperature reduction), the net power of the organic part of Rankine was increased in the constant conditions of pinch and approach temperature. The increase in the combustion gases led to the production of organic fluid discharge, finally leading to power generation in the ORC system.

Fig. 11 shows the heat loss from the gas turbine exhaust. Approximately 560 and 630 MW heat exited from the gas turbine exhaust. As the ambient temperature was increased, the temperature of the exhaust gas from the gas turbine was enhanced. As a result, it could be seen in this figure that the mass flow rate played a more important role in comparison to the temperature changes of exhaust gas from the gas turbine. This was such that this trend could be seen by drawing the variation of heat loss from the turbine in terms of the temperature of the exhaust gas from the gas turbine.

Fig. 12 shows the thermo-economic evaluation of the investigated cycle with ORC. It could be observed that the annual costs of the ORC system were reduced by increasing the ambient temperature. The cost of the ORC system was composed of four main components. In Fig. 13, the percentage of part of each equipment cost can be seen. As shown, the heat recovery boiler assigned the greatest cost in the ORC with different fluids to itself. Fig. 13 shows the trend of changes in the cost of the heat recovery boiler design at various ambient temperatures.

It could be observed that by increasing the flow rate of the combustion gasses, the costs of making recovery boiler were increased significantly and the trend of this increase affected the annual costs of the ORC system; also, the trend of its changes was affected by the costs of the heat recovery boiler.

According to changes in the price of the power generated from the ORC system, it could be found that using the recycled output gas led to the reduction of the power cost, as compared to the power produced by a gas turbine. Also, Fig. 14 shows that as the ambient temperature was increased, the price of the generated power was raised. This could be suitable due to the reduction of the organic cycle turbine production as a result of the reduction in the flow rate of the working cycle. The reduction of the combustion gases at high temperatures led to a less production flow rate in the heat recovery boiler, which could increase the price of the produced power.

Two important parameters in the ORC system with constant pinch and approach conditions in HRSG are the cost of the power generated by the organic cycle turbine and the system energy efficiency. Therefore, in this study, these

Table 13  
Input parameters for the economic analysis of the system [35]

Parameter	Value
System total capacity factor ( $f_c$ )	0.9
Price of each membrane, cm[\$]	1,000; 1,200; and 1,400 depending on its type
Inflation, %	10
Operation life, y	20
8-inch pressure vessel	1,000
Electricity, \$/kWh	0.08

Table 14  
Results of ORC cycle validation according to the reference [33]

Parameter	Present study	Reference
Evaporator duty, kW	252	252
Condenser duty, kW	196.0	194.6
Turbine power, kW	62	61
Pump power, kW	4.06	3.46
Net power, kW	57.94	57.54
Thermal efficiency, %	22.99	22.83
Mass flow (organic fluid), kg/s	1.96	1.91

Table 15  
Results obtained from validation using the ROSA software

Parameter	Simulation results	Results from ROSA	Error (%)
Salt concentration of the treated water produced in stage 1 (ppm)	20.94	23.50	10
Salt concentration of the freshwater produced in stage 2 (ppm)	55.82	65.58	14
Water produced in stage 1 (m <sup>3</sup> /h)	40.12	40.83	1.7
Water produced in stage 2 (m <sup>3</sup> /h)	19.87	19.17	3.6
Feed pressure (MPa)	3.33	3.77	11.6
Water recovery (%)	75.0	75.0	0

Table 16  
Results of the MED system validation

Parameter	Freshwater production (m <sup>3</sup> /d)
Simulation data	1,536
Reference data [6]	1,557
Difference (%)	1.35

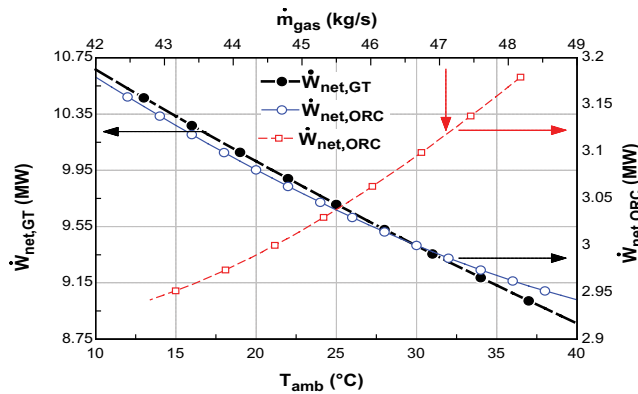


Fig. 10. Changes in gas turbine net power and the organic Rankine turbine in terms of ambient air temperature and the flow rate of the exhaust gas from the gas turbine.

two important parameters were analyzed. Fig. 15 shows the results of the working fluid variation on these two important cycle parameters. Among the mentioned organic fluids, it could be observed that R141b and R123 had lower costs and higher efficiency, as compared to other working fluids. Additionally, in these two fluids, R141b had more appropriate conditions, such that its cycle had an efficiency of 16.6% and the approximate cost of 0.048 \$/kWh.

By using Table 4, this part is analyzed; this explains why the R141b working fluid had a lower cost and efficiency. According to this table, it could be found that the cycle thermal efficiency was completely a function of temperature and critical pressure. It was found that by considering the high temperature of combustion gases, the working fluids R141b and R123 had the highest thermal efficiency and the appropriate price of the generated power.

According to Fig. 5 flowchart, which indicates the working fluid selection, Fig. 15 shows that the working fluid R123 had the appropriate thermal efficiency and price of generated

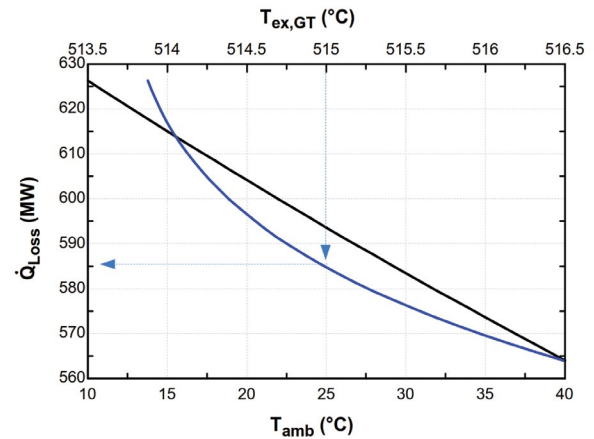


Fig. 11. Variation of heat loss from the gas turbine exhaust in terms of the temperature of the exhaust gas from the gas turbine.

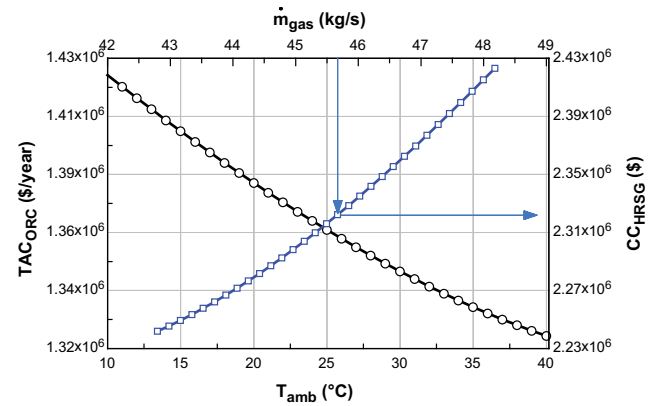


Fig. 12. Variation in the annual costs of ORC and the cost of HRSG purchase with ambient temperature and the flow rate of the exhaust gas from the gas turbine.

power, and with better environmental conditions in comparison to other fluids. The global warming potential (GWP) of the fluid R141b was very higher than that of R123; therefore, R123 could be suggested as a working fluid for the organic cycle.

One of the important parameters is the UPC. A large part of the system's costs depends on the current system costs, including the high-pressure RO pumps; therefore, with the constant consumed power, the greater the production, the

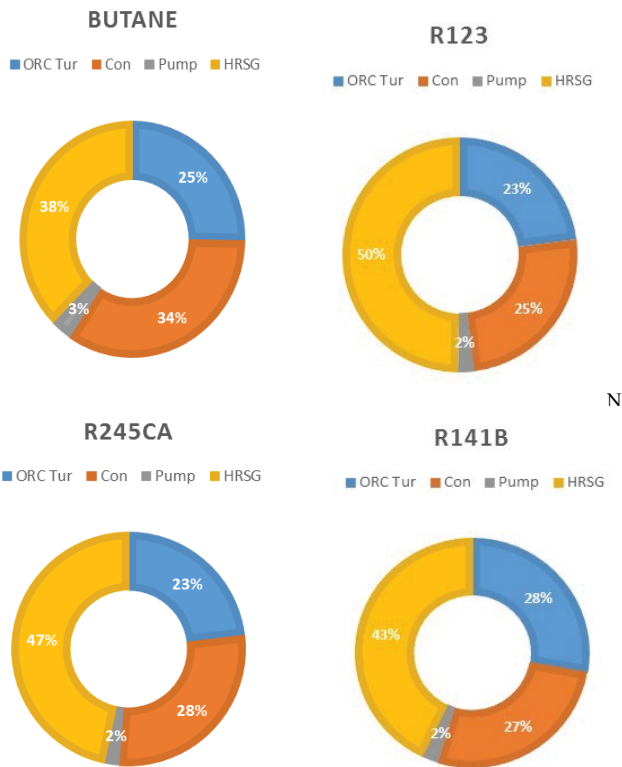


Fig. 13. Cost percentage of each component of the total costs of purchasing the ORC equipment for various fluids.

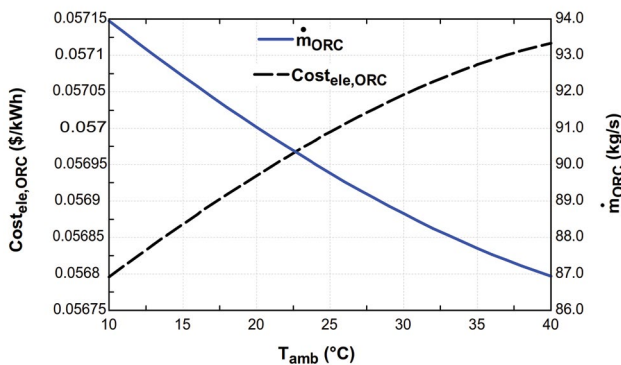


Fig. 14. Variation in the price of the power produced from the ORC system with the ambient temperature and the flow rate of the working fluid produced in HRSG.

lower the cost of the produced water. In high sea concentrations, the price of electricity is increased due to the lower production. Fig. 16 shows the effect of changing the type of working fluid on the water produced from the power of ORC. As could be observed, the increased production power led to enhanced freshwater production, causing the water cost to be reduced. However, as mentioned before, the environmental impacts of the R123 fluid were less than those of other fluids investigated in this research; it had more appropriate efficiency and power cost, as compared to other fluids.

Under the same conditions, if gas turbine power is used to produce freshwater (i.e., 30% of the production power is

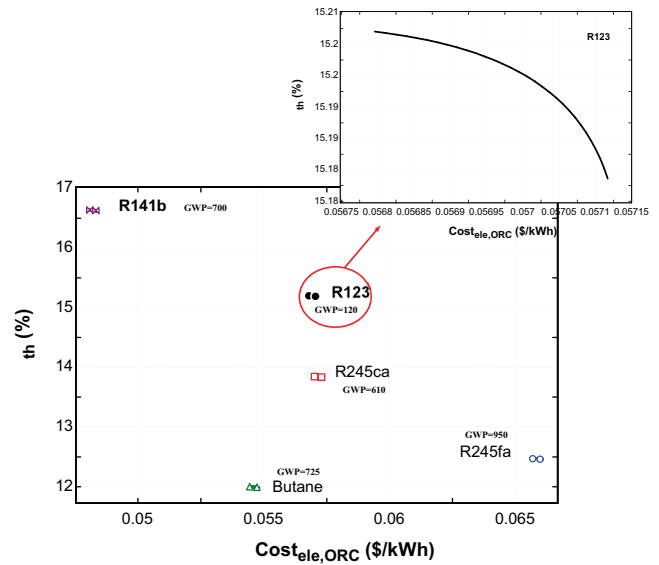


Fig. 15. Effect of the working fluid type changes on the price and efficiency of the first thermodynamic law.

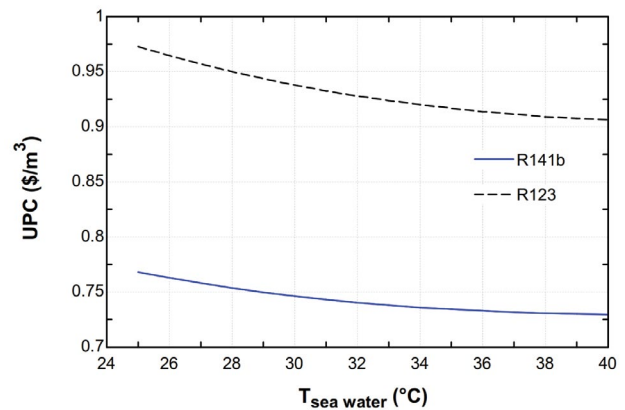


Fig. 16. Effect of changing the type of working fluid in the ORC system on the produced freshwater price in the Persian Gulf water concentration.

assigned to freshwater), it can be, therefore, found that the cost of the produced water-based on the gas turbine system may be greater than that of the ORC system. The prices will be different by 0.4 \$/m<sup>3</sup>. The reason is that the cost of the produced power for the gas turbine increases the operational costs. The difference between the annual costs of gas turbines and RO with ORC and RO cycle can be seen in Fig. 17. As shown, the costs of ORC + RO are less than those of GT + RO.

Another scenario regarding the freshwater production in a gas turbine is how the cost of water in gas turbines powers is assigned to the RO system pump. Therefore, in this part, a fraction of power assigned to the RO system ( $F_{RO}$ ) is considered to be variable. According to Fig. 18, it could be observed that by increasing the assigned power, the recovery rate was raised. As the rate of recovery was increased, the quality of the produced freshwater showed a downward trend, and the conflict between  $J_s$  and  $V_w$  parameters led to

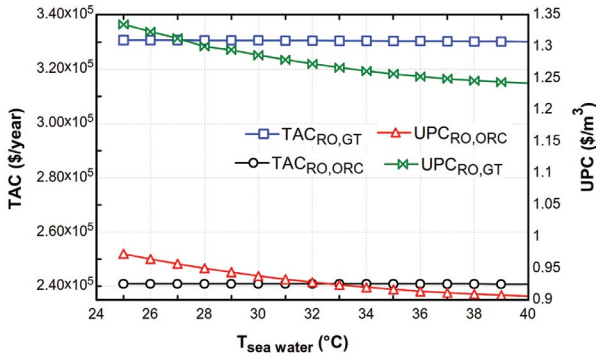


Fig. 17. Comparison of the cost of the produced water and the annual costs of GT + RO and ORC + RO.

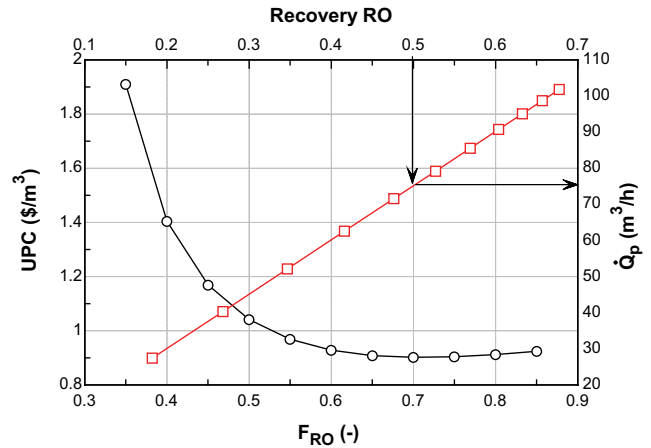


Fig. 19. Changes in the price of the produced water and the flow rate of freshwater by recovery of the specific fraction of power.

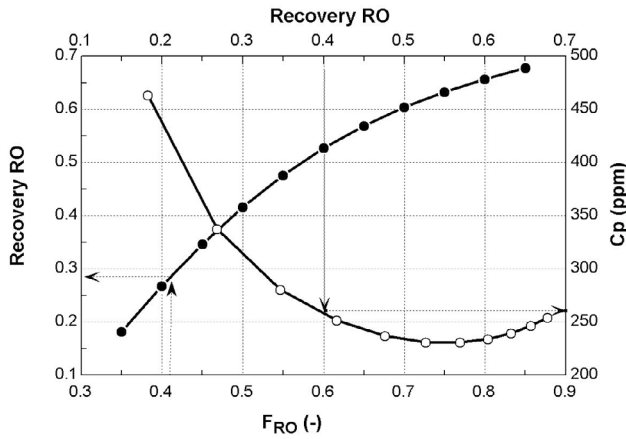


Fig. 18. Changes in the recovery and concentration of the produced freshwater in terms of the fraction gas turbine power assigned to the RO system.

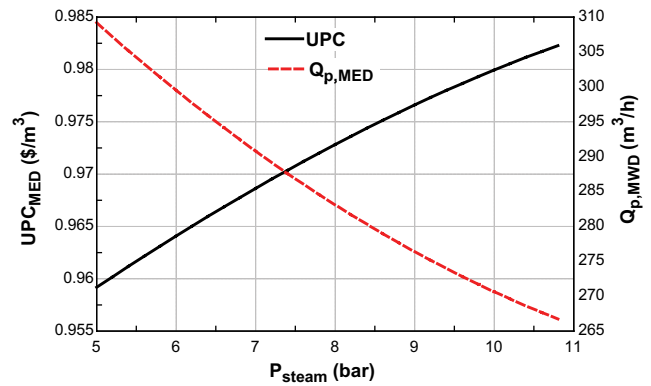


Fig. 20. Changes in the cost of the produced water from the MED system and the amount of the produced fresh water.

the occurrence of concavity in the above recoveries. One of the important parameters of water price is the amount of produced water. In Fig. 19, it can be observed that the power price was decreased as the freshwater production was increased; at high pressures, the operational costs could have a greater influence on the price, and costs are increased due to the increase in pressure and the lack of increase in water proportional to the increase in the rate of pressure.

In this section, the change of technology type, that is, the heat of the exhaust gas from the gas turbine to produce steam and desalinate saline water in a multi-effect system is discussed. In this case, the effect of changing the technology type on the price of water production will be investigated. This comparison can finally determine which technology in freshwater production can both increase production and minimize the final price of freshwater. Here, a heat recovery boiler was placed in the outlet of the gas turbine exhaust, which produced 8.5 bar vapor in a saturated state. This vapor was used as a stimulator for the MED system.

Fig. 20 shows the water cost for the MED system based on the pressure variation of the vapor entering it. As pressure was increased, the flow rate of the produced vapor was decreased; as a result, the flow rate of the produced

freshwater was decreased. This affected the cost of fresh water in the MED system and increased it.

Fig. 21 shows the changes in the price of the produced freshwater together with the GOR of the MED system; changes in effects were investigated as well. It could be observed that by increasing the number of effects, the price of the produced fresh water was decreased and GOR was increased.

Finally, it was found for which desalination systems the cost of water in the gas turbine-based freshwater production could be suitable. Based on two designs, Table 17 shows the flow rate of freshwater. In this design, the total produced power of gas turbine and the ORC system with the working fluid R123 has been assigned to the RO system. In the MED system, the saturated vapor of 8.5 bar has been considered for a 4-effect exchanger, as commonly done.

In another analysis, a fraction of the exhaust gas from the turbine entered into the ORC system, and another part entered into the MED system and its heat recovery boiler. According to Fig. 22, it could be seen that by increasing the part of exhaust gases toward the ORC system, the amount of the produced water was increased and the freshwater production was decreased, such that the price of freshwater was raised from 0.98 \$ to 1.06 \$/m<sup>3</sup>.

By identifying the organic fluid R123 in the upstream gas turbine cycle in terms of power and environmental impacts, the compression cooling system could be analyzed by keeping the working fluid constant in this analysis. Additionally, in the gas turbine cycle, different analyses were conducted on this system, as shown in the previous parts, and the system and its components were well identified. As the compression cooling system has a direct relationship with the compressor power, the compressor gets its power from these two cycles; therefore, it could be found that each factor affecting the ORC system power and GT will also directly influence cooling.

Thermal load changes of the compression cooling cycle, which are working with ammonia fluid at the ambient

temperature, can be seen in Fig. 23. In this modeling, it was assumed that the temperature of the hot source was equal to the ambient temperature and the temperature of the cold source was 260°K. In this analysis, it was found that by increasing the ambient temperature, the cooling load was reduced. This was due to both the reduction of turbine power and the ORC section and the increase in the hot source, which had no linear trend of changes. The increased temperature reduced the whole system’s cooling power from 55 to 30 MW. As can be seen, about 80% of cooling power was supplied through the gas turbine and the rest was supplied from the ORC system.

Moreover, it could be observed in Fig. 24 that by increasing the ambient temperature, the compression system efficiency or the system function coefficient was reduced. The reason was the reduction of the absorbed heat from the operator. Though the produced power was also reduced,  $\dot{Q}_{Eva}$  was greater than the received power, and this could be found from the decreasing trend of COP. On the other hand, as this system had a high consumption power, it assigned a large part of the operational costs to itself. Therefore, by decreasing the received power, the current costs of the system were reduced.

By considering the exhaust gas from the gas turbine, the cooling load could be produced using this heat; by using a

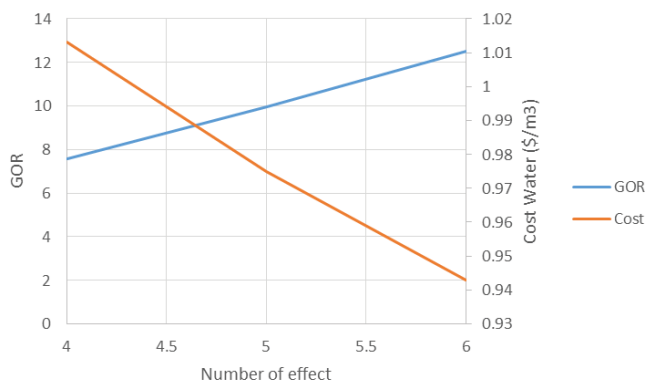


Fig. 21. Changes in the cost of the produced water from the MED system and GOR with changes in the number of effects.

Table 17  
Comparison of two water desalination systems in terms of water production and the cost of the produced water

Desalination water system	Produced flow rate (m <sup>3</sup> /h)	Cost of water (m <sup>3</sup> /)\$)
RO system	194	0.943
System MED	213	1.01

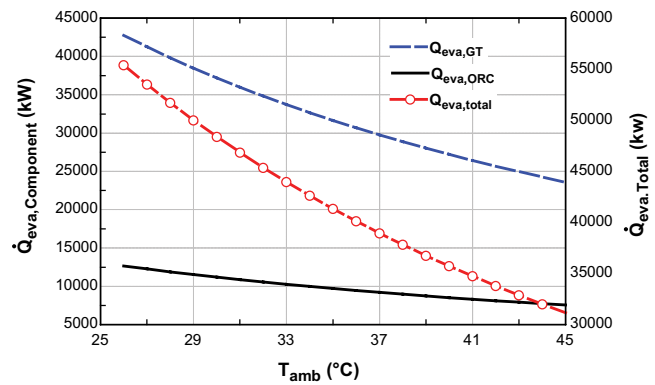


Fig. 23. Variation of  $\dot{Q}_{Eva}$  in each component and the general state with variation at the ambient temperature in the compression chiller.

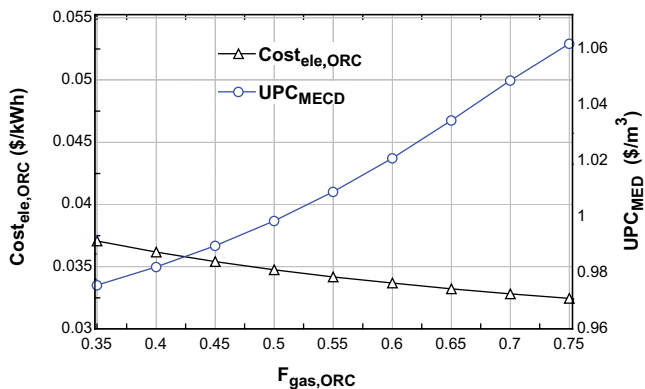


Fig. 22. Changes in the price of the ORC produced power and the water price of the MED system by assigning the part of the exhaust gas from the turbine.

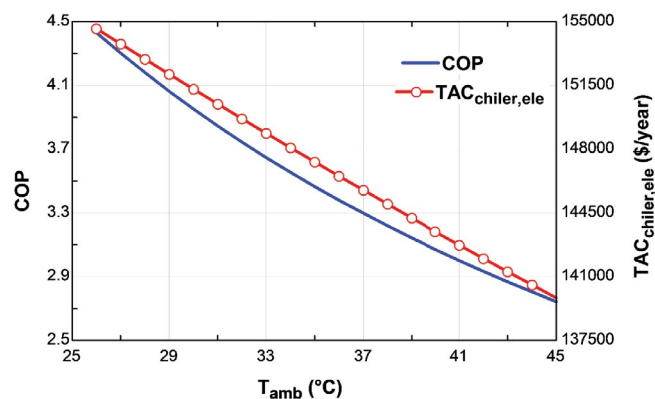


Fig. 24. Changes in COP and TAC with the ambient temperature in the compression chiller.

single effect, the lithium bromide (LiBr) absorption chiller with COP = 0.72 is obtained.

Only its consumed fuel for its generator part was considered as one of the current costs, which caused an increase of costs; however, by using the exhaust gas from the gas turbine in this scenario, the only current costs were the system repair and the maintenance costs. Therefore, in comparison to the compression system, this system could have very lower annual costs. Fig. 25 shows the results of this investigation. By increasing the ambient temperature, the amount of COP was considered to be constant because the

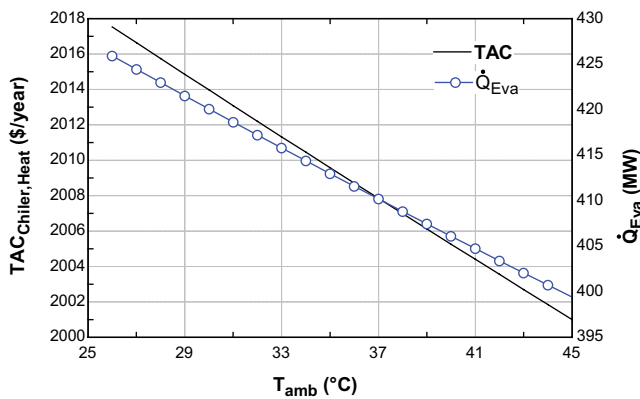


Fig. 25. Changes in the amount of cooling load in the absorption chiller and its annual costs in terms of the ambient temperature.

absorption chillers were less influenced by the environment, in comparison to the compression chillers. The reason was that they had a cooling water system (wet tower) which had small variations with ambient temperature. Additionally, in the previous sections, it was observed that the turbine outlet temperature showed small temperature variations and these changes were not tangible. Given this assumption, it could be seen that the amount of the cooling load was very greater than that of compression chillers and its annual costs also had a tangible reduction.

The results of this analysis showed that the use of the exhaust gas for cooling by the absorption chiller could be very suitable from the energy and economic perspective, reducing as costs, compared to a compression system.

#### 4. Conclusions

The energy and economic analysis of the freshwater production system showed that the MED system was capable of producing a high tonnage freshwater with a price of approximately 1 \$/m<sup>3</sup>. To produce this amount of freshwater from the RO system, the whole capacity of the gas turbine and ORC system should be used so that a production similar to the MED system could be obtained, but the cost of the produced freshwater from this system might be less than that of MED, equal to 0.94 \$/m<sup>3</sup>. Therefore, if the high tonnage is required for water desalination, the MED system should be used; if it is not intended to produce a high amount of freshwater and it is important in terms of economic issues, the use of production power in the ORC section will reduce the current costs

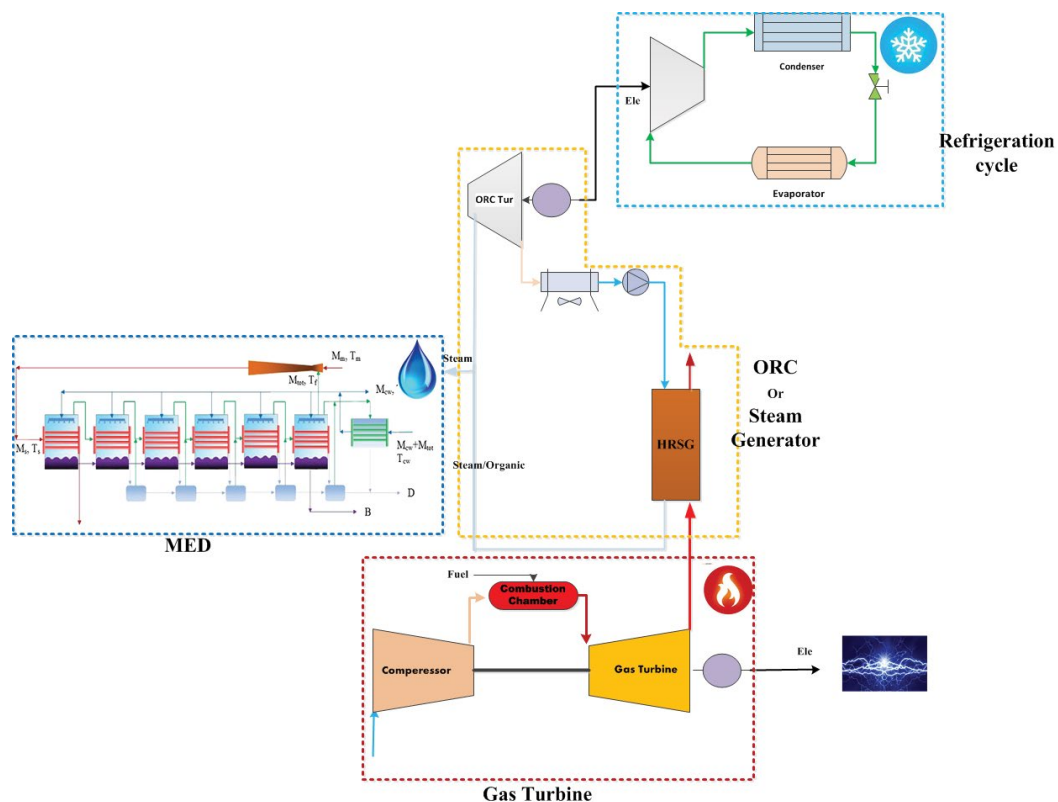


Fig. 26. Schematic of the proposed cycle for high tonnage water, low-temperature cooling, and power sale.

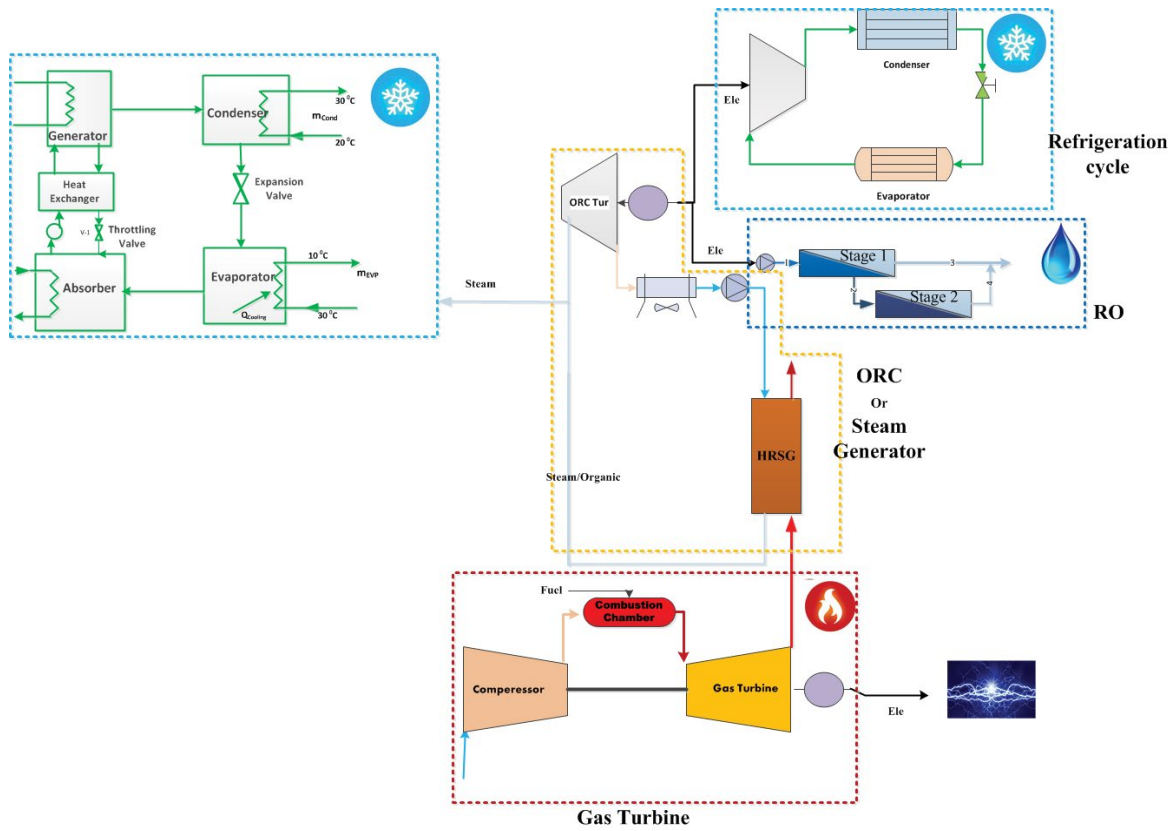


Fig. 27. Schematic of the proposed cycle for the power sale, low-temperature cooling and high tonnage along with economical fresh-water production.

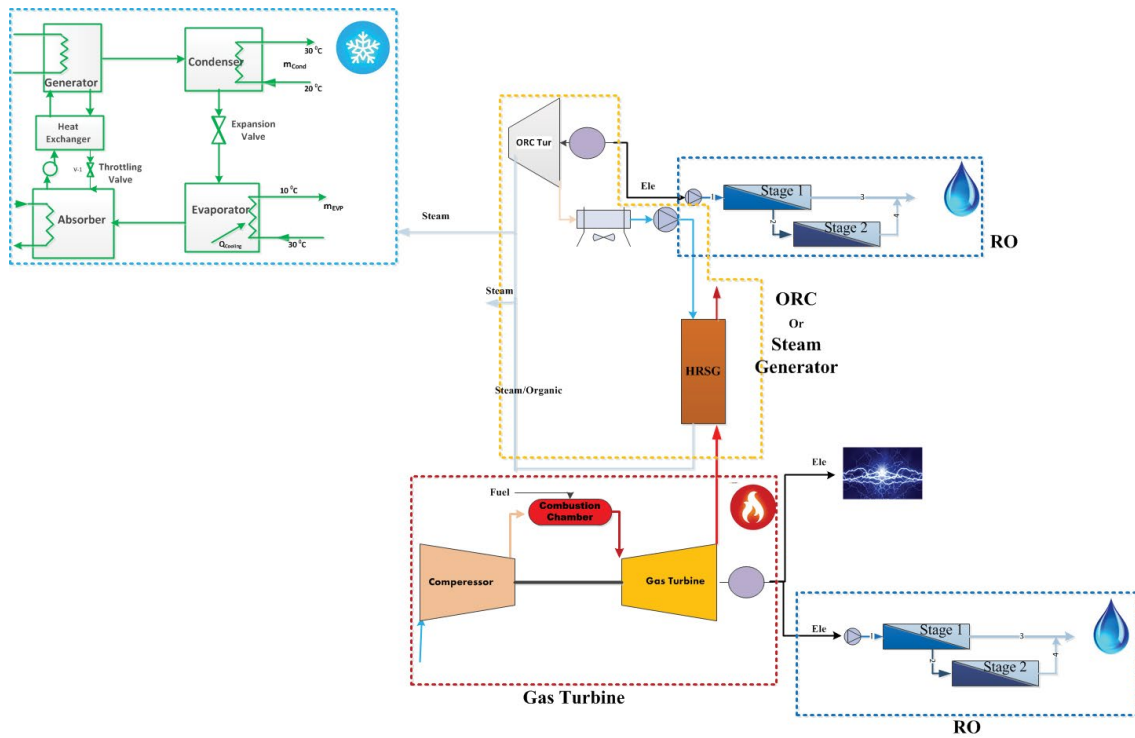


Fig. 28. Schematic of the proposed cycle for the high tonnage freshwater and its reasonable price, along with high and economical tonnage of cooling and sale of electricity.

Table 18

Results of the proposed cycles based on the combined power, freshwater and cooling production

Proposed schematic	Power	Cooling	Water
Fig. 26	Power sale (GT)	Need for low-temperature cooling (compression system)	High freshwater tonnage (MED)
Fig. 27	Power sale (GT)	High cooling load (absorption chiller)	Reasonable water price and limited tonnage (RO)
Fig. 28	Power sale (GT)	High cooling tonnage (absorption chiller)	High-tonnage freshwater at reasonable prices (RO)

of the RO system in comparison to GT, and it is economical to use the ORC system for this purpose.

Given that the cost of the power produced by the gas turbine from the ORC cycle is higher, for network sale, the use of GT power can increase the profit, and the use of the ORC power for uses such as freshwater production is suitable; also, in special circumstances (such as reaching low temperatures ranging from  $-12^{\circ}\text{C}$  to  $-20^{\circ}\text{C}$ ), condensing systems should be used because the power produced in the ORC system has a lower price than the GT cycle. The results of this study, therefore, showed that the use of the exhaust gas for cooling by the absorption chiller could be very suitable from an energy and economic perspective, and the costs could be reduced when compared to a compression system.

Additionally, in the ORC, the working fluids R123 and R141b were selected as the fluids with high thermal efficiency and lower price of the produced power. According to the flowchart presented in this paper, the R123 fluid was selected due to its less environmental impacts (GWP).

Therefore, the graphic conclusion of the present work could be summarized in Table 18 based on the existing conditions.

### Symbols

AFUDC	—	Allowance for the funds used during construction, \$
AOC	—	Annual operational costs, year/\$
$B$	—	Solute transport coefficient, $\text{kg}/\text{m}^2 \text{ s}$
$C_f$	—	Concentration, ppm
CRF	—	Capital recovery factor
$D$	—	Feed channel equivalent diameter, mm
$D_s$	—	Solute diffusivity, $\text{m}^2/\text{s}$
$D$	—	Freshwater discharge, $\text{kg}/\text{s}$
DC	—	Direct costs, \$
$F$	—	Feed water mass flow rate, $\text{kg}/\text{s}$
FCI	—	Fixed capital investment, \$
GOR	—	Gain output ratio
GWP	—	Global warming potential
$I$	—	Inflation rate, %
IC	—	Indirect cost, \$
$J_s$	—	Local solute flux, $\text{kg}/\text{m}^2 \text{ s}$
$J_w$	—	Local permeate flux, $\text{kg}/\text{m}^2 \text{ s}$
$K$	—	Local mass transfer coefficient
LRD	—	Licensing, research and development costs, \$
$L_m$	—	Membrane length, m
$N_i$	—	Number of plates
$N$	—	Number of elements
ONSC	—	Including onsite costs, \$

OFSC	—	Offsite costs, \$
ODP	—	Ozone depleting potential
OC	—	Operating costs, \$
$Q$	—	Flow rate, $\text{kg}/\text{s}$
Re	—	Reynolds number
$S$	—	Injection vapor pressure, $\text{kg}/\text{s}$
Sc	—	Schmidt number
SUC	—	Startup costs, \$
$T$	—	Temperature, $^{\circ}\text{C}$
TAC	—	Total annual cost, \$
UPC	—	Unit product cost, $\text{m}^3/\text{\$}$
$V_w$	—	Permeate velocity, $\text{m}/\text{s}$
WC	—	Working costs, \$

### Greek letters

$\rho$	—	Density, $\text{kg}/\text{m}^3$
$\mu$	—	Liquid viscosity, Pa s
$\pi$	—	Local osmotic pressures of the solutions, MPa

### Subscript

$B$	—	Brine stream
$F$	—	Feed stream
$P$	—	Permeate stream
$W$	—	Membrane wall

### References

- [1] R. Salcedo, E. Antipova, D. Boer, L. Jiménez, G. Guillén-Gosálbez, Multi-objective optimization of solar Rankine cycles coupled with reverse osmosis desalination considering economic and life cycle environmental concerns, *Desalination*, 286 (2012) 358–371.
- [2] K. Ansari, H. Sayyaadi, M. Amidpour, A comprehensive approach in optimization of a dual nuclear power and desalination system, *Desalination*, 269 (2011) 25–34.
- [3] Y.S.H. Najjar, A.M. Abubaker, A.F.S. El-Khalil, Novel inlet air cooling with gas turbine engines using cascaded waste-heat recovery for green sustainable energy, *Energy*, 93 (2015) 770–785.
- [4] G. Iaquaniello, A. Salladini, A. Mari, A.A. Mabrouk, H.E.S. Fath, Concentrating solar power (CSP) system integrated with MED-RO hybrid desalination, *Desalination*, 336 (2014) 121–128.
- [5] M.H.K. Manesh, H. Ghalami, M. Amidpour, M.H. Hamed, Optimal coupling of site utility steam network with MED-RO desalination through total site analysis and exergoeconomic optimization, *Desalination*, 316 (2013) 42–52.
- [6] H. Mokhtari, M. Sepahvand, A. Fasihfar, Thermoeconomic and exergy analysis in using hybrid systems (GT + MED + RO) for desalination of brackish water in Persian Gulf, *Desalination*, 399 (2016) 1–15.

- [7] H. Mokhtari, M. Bidi, M. Gholinejad, Thermo-economic analysis and multiobjective optimization of a solar desalination plant, *J. Sol. Energy*, 2014 (2014) 13 pages, <https://doi.org/10.1155/2014/892348>.
- [8] S. Loutatidou, H.A. Arafat, Techno-economic analysis of MED and RO desalination powered by low-enthalpy geothermal energy, *Desalination*, 365 (2015) 277–292.
- [9] G. Filippini, M.A. Al-Obaidi, F. Manenti, I.M. Mujtaba, Performance analysis of hybrid system of multi effect distillation and reverse osmosis for seawater desalination via modelling and simulation, *Desalination*, 448 (2018) 21–35.
- [10] M. Salimi, M. Amidpour, Investigating the integration of desalination units into cogeneration systems utilizing R-curve tool, *Desalination*, 419 (2017) 49–59.
- [11] S. Ud-Din Khan, S. Ud-Din Khan, Karachi Nuclear Power Plant (KANUPP): as case study for techno-economic assessment of nuclear power coupled with water desalination, *Energy*, 127 (2017) 372–380.
- [12] S. Ihm, O.Y. Al-Najdi, O.A. Hamed, G. Jun, H. Chung, Energy cost comparison between MSF, MED and SWRO: case studies for dual purpose plants, *Desalination*, 397 (2016) 116–125.
- [13] A.M.A. Arani, V. Zamani, A. Behbahaninia, Economic analysis of a combined power and desalination plant considering availability changes due to degradation, *Desalination*, 414 (2017) 1–9.
- [14] S.R. Hosseini, M. Amidpour, S.E. Shakib, Cost optimization of a combined power and water desalination plant with exergetic, environment and reliability consideration, *Desalination*, 285 (2012) 123–130.
- [15] S. Sanaye, S. Asgari, Four E analysis and multi-objective optimization of combined cycle power plants integrated with multi-stage flash (MSF) desalination unit, *Desalination*, 320 (2013) 105–117.
- [16] B. Ghorbani, M. Mehrpooya, H. Ghasemzadeh, B. Ghorbani, M. Mehrpooya, H. Ghasemzadeh, Investigation of a hybrid water desalination, oxy-fuel power generation and CO<sub>2</sub> liquefaction process, *Energy*, 158 (2018) 1105–1119.
- [17] B. Ghorbani, M. Mehrpooya, M. Sadeghzadeh, Developing a tri-generation system of power, heating, and freshwater (for an industrial town) by using solar flat plate collectors, multi-stage desalination unit, and Kalina power generation cycle, *Energy Convers. Manage.*, 165 (2018) 113–126.
- [18] M. Mehrpooya, B. Ghorbani, S.S. Hosseini, Thermodynamic and economic evaluation of a novel concentrated solar power system integrated with absorption refrigeration and desalination cycles, *Energy Convers. Manage.*, 175 (2018) 337–356.
- [19] M.W. Shahzad, M. Burhan, K.C. Ng, Pushing desalination recovery to the maximum limit: Membrane and thermal processes integration, *Desalination*, 416 (2017) 54–64.
- [20] M.S. Azhar, G. Rizvi, I. Dincer, Integration of renewable energy based multigeneration system with desalination, *Desalination*, 404 (2017) 72–78.
- [21] A. Nemati, M. Sadeghi, M. Yari, Exergoeconomic analysis and multi-objective optimization of a marine engine waste heat driven RO desalination system integrated with an organic Rankine cycle using zeotropic working fluid, *Desalination*, 422 (2017) 113–123.
- [22] Y.S.H. Najjar, A.M. Abubaker, Thermo-economic analysis and optimization of a novel inlet air cooling system with gas turbine engines using cascaded waste-heat recovery, *Energy*, 128 (2017) 421–434.
- [23] P. Ahmadi, I. Dincer, Thermodynamic analysis and thermo-economic optimization of a dual pressure combined cycle power plant with a supplementary firing unit, *Energy Convers. Manage.*, 52 (2011) 2296–2308.
- [24] M. Ameri, H. Mokhtari, M.M. Sani, 4E analyses and multi-objective optimization of different fuels application for a large combined cycle power plant, *Energy*, 156 (2018) 371–386.
- [25] A.M. Nabati, M.S. Sadeghi, S.N. Naserabad, H. Mokhtari, S. Izadpanah, Thermo-economic analysis for determination of optimized connection, *Energy*, 162 (2018) 1062–1076.
- [26] H. Mokhtari, H. Ahmadisedigh, M. Ameri, the optimal design and 4E analysis of double pressure HRSG utilizing steam injection for Damavand power plant between solar field and combined cycle power plant, *Energy*, 118 (2017) 399–413.
- [27] H. Mokhtari, A. Esmaili, H. Hajabdollahi, Thermo-economic analysis and multiobjective optimization of dual pressure combined cycle power plant with supplementary firing, *Heat Transfer Asian Res.*, 45 (2016) 59–84.
- [28] P. Ahmadi, M.A. Rosen, I. Dincer, Greenhouse gas emission and exergo-environmental analyses of a trigeneration energy system, *Int. J. Greenhouse Gas Control*, 5 (2011) 1540–1549.
- [29] A. Baghernejad, M. Yaghoubi, Exergoeconomic analysis and optimization of an integrated solar combined cycle system (ISCCS) using genetic algorithm, *Energy Convers. Manage.*, 52 (2011) 2193–2203.
- [30] A. Esmaili, P. Keshavarz, M.S. Ehsan Shakib, M. Amidpour, Applying different optimization approaches to achieve optimal configuration of a dual pressure heat recovery steam generator, *Int. J. Energy Res.*, 37 (2012) 1440–1452.
- [31] A. Bejan, G. Tsatsaronis, M.J. Moran, M. Moran, *Thermal Design and Optimization*, Wiley Interscience, John Wiley Sons Inc., New York, 1996.
- [32] V. Ganapathy, *Industrial Boilers and Heat Recovery Steam Generators Design, Applications, and Calculations*, Marcel Dekker, Inc., New York, 2003.
- [33] S. Safarian, F. Aramoun, Energy and exergy assessments of modified organic Rankine cycles (ORCs), *Energy Rep.*, 1 (2015) 1–7.
- [34] Y.A. Cengel, M.A. Boles, *Thermodynamics, an Engineering Approach*, 6th ed., McGraw Hill, New York, NY, 2007.
- [35] H. Mokhtari, H. Ahmadisedigh, I. Ebrahimi, Comparative 4E analysis for solar desalinated water production by utilizing organic fluid and water, *Desalination*, 377 (2016) 108–122.
- [36] M. Khanarmuei, H. Ahmadisedigh, I. Ebrahimi, L. Gosselin, H. Mokhtari, Comparative design of plug and recirculation RO systems; thermo-economic: case study, *Energy*, 121 (2017) 205–219.
- [37] N.M. Al-Bastaki, A. Abbas, Predicting the performance of RO membranes, *Desalination*, 132 (2000) 132–187.
- [38] J. Esfahani, C.K. Yoo, Feasibility study and performance assessment for the integration of a steam-injected gas turbine and thermal desalination system, *Desalination*, 332 (2014) 18–32.
- [39] Y.S.H. Najjar, A.M. Abubaker, Indirect evaporative combined inlet air cooling with gas turbines for green power technology, *Int. J. Refrig.*, 59 (2015) 235–250.
- [40] B. Prasartkaew, Performance test of a small size LiBr-H<sub>2</sub>O absorption chiller computer modeling of a single-stage lithium bromide/water absorption refrigeration unit, *Energy Procedia*, 56 (2014) 487–497.
- [41] H. Mokhtari, H. Hadiannasab, M. Mostafavi, A. Ahmadibeni, B. Shahriari, Determination of optimum geothermal Rankine cycle parameters utilizing, *Energy*, 102 (2016) 260–275.
- [42] H. Hajabdollahi, Evaluation of cooling and thermal energy storage tanks in optimization of multi-generation system, *Energy Storage*, 4 (2015) 1–13.

## Appendix

### A1. Price of the organic Rankine cycle (ORC) system and cooling systems equipment

As the organic Rankine cycle (ORC) system is composed of different equipment, each of the equipment cost is shown in Table A1.

Table A1  
Proposed relations used to determine the price of the ORC system [33,41]

Equipment	Equation
Turbine	$Z_{ST} = a_1 w^{a_2} \phi_{\eta_1} \cdot \phi_T$ $\phi_{\eta_1} = 1 + \left( \frac{1 - \bar{\eta}_1}{1 - \eta_1} \right)^{a_3}$ $\phi_T = 1 + a_4 \cdot \exp\left(\frac{T_1 - \bar{T}_1}{a_5}\right); a_1 = 3880.5 \frac{\$}{\text{KW}^{0.7}}; a_2 = 0.5; a_3 = 3; a_4 = 5; a_5 = 10.42; \bar{\eta}_1 = 0.95; \bar{T}_1 = 866; \eta_1 = 0.9$ <span style="float: right;">(A1)</span>
Pump	Similar to the reverse osmosis pump
Condenser	$Z_{Con} = \frac{a_1 \dot{Q}_{Con}}{k \cdot \Delta T_{in}} + a_2 \dot{m}_m + 70.5; \dot{Q}_{con} \times (-0.6936 \ln(\bar{T}_{cw} - T_b) + 2.1897)$ $a_1 = 280.74 \$ \cdot \text{m}^{-2}; a_2 = 746 \$ (\text{Kg s})^{-1} k = 2,200$ <span style="float: right;">(A2)</span>

In this table,  $\phi_{\eta_1}$  is the efficiency correction factor of the first law and  $\phi_T$  is the correction factor of the inlet vapor temperature.

### A2. Absorption and compression chiller

The initial cost of absorption and the electrical cost is evaluated using the following relations [42]:

$$C = 540 (\text{CH}_{\text{nom,ab}})^{0.872} \quad (\text{A3})$$

$$C = 482 (\text{CH}_{\text{nom,el}})^{0.93} - 159.7 (\text{CH}_{\text{nom,el}}) \quad (\text{A4})$$